Next-to-leading order effects on the lightest scalar tetraquark mass estimates using QCD Laplace sum-rules

A thesis submitted to the
College of Graduate and Postdoctoral Studies
in partial fulfillment of the requirements
for the degree of Master of Science
in the Department of Physics and Engineering Physics
University of Saskatchewan
Saskatoon

By
Bárbara Cid Mora

Permission to Use

In presenting this thesis in partial fulfillment of the requirements for a Postgraduate degree from the University of Saskatchewan, I agree that the Libraries of this University may make it freely available for inspection. I further agree that permission for copying of this thesis in any manner, in whole or in part, for scholarly purposes may be granted by the professor or professors who supervised my thesis work or, in their absence, by the Head of the Department or the Dean of the College in which my thesis work was done. It is understood that any copying or publication or use of this thesis or parts thereof for financial gain shall not be allowed without my written permission. It is also understood that due recognition shall be given to me and to the University of Saskatchewan in any scholarly use which may be made of any material in my thesis.

Disclaimer

Reference in this thesis to any specific commercial products, process, or service by trade name, trademark, manufacturer, or otherwise, does not constitute or imply its endorsement, recommendation, or favoring by the University of Saskatchewan. The views and opinions of the author expressed herein do not state or reflect those of the University of Saskatchewan, and shall not be used for advertising or product endorsement purposes.

Requests for permission to copy or to make other uses of materials in this thesis in whole or part should be addressed to:

Department of Physics & Engineering Physics
University of Saskatchewan
116 Science Place, Rm 163
Saskatoon, SK S7N 5E2
Canada

OR

Dean

College of Graduate and Postdoctoral Studies

University of Saskatchewan

116 Thorvaldson Building, 110 Science Place

Saskatoon, Saskatchewan S7N 5C9 Canada

Abstract

Multiquark states have been of great interest among hadronic physicists, and despite the big breakthrough that came in 2003 with the discovery of the charmonium-like tetraquark candidate $X(3872)$, their structure and masses are still eclipsed by theoretical uncertainties in the precision of the calculations. The study of tetraquarks can give us another insight to understand strong interactions at the elementary level and at different energy scales. The goal of this research is to explore light-quark tetraquark structures and estimate their masses using the QCD sum-rules approach. The specific focus is on the controversial light scalar tetraquark σ (denoted as $f_0(500)$ in the Particle Data Group classification scheme), and the contributions from next-to-leading order (NLO) diagrams to the spectral functions are incorporated in the process of finding a Borel window for a reliable sum-rule analysis. After a deep examination, this thesis includes analyses in terms of a single and a double resonance models, where the heavier state (980 MeV) used is the scalar $f_0(980)$. The results showed that the NLO terms play a significant role in the spectral function picture with contributions of up to 74% with respect to the leading-order (LO) perturbative terms, but their effects are suppressed in ratios used within the Laplace sum-rules scheme. Moreover, the key improvement is that NLO corrections benefit substantially the methodology by locating a suitable physical Borel window where the mass prediction range is reliable and result in the σ mass prediction around $0.52\,\text{GeV} < m_\sigma < 0.69\,\text{GeV}$. It was also found that the relative strength of the $f_0(980)$ coupling to the current is approximately three to four times stronger than the σ, such results are in agreement with chiral Lagrangian determinations, hence in accordance with the tetraquark scheme.

Acknowledgements

Thanks to Professor Tom Steele, who guided not only my life as a MSc student, but also motivated me to be a better scientist and to challenge myself in many aspects of life. Thanks for all your advice and guidance. Working with you was an amazing experience, I am lucky that I had you as a mentor. In this sense, thanks to Professor Marcelo Loewe for all the support and advice, for which I am where I am. Finally, thanks to the advisory committee, Professors Steven Rayan and Adam Bourassa for their great insights and interesting comments on the thesis. Specially Professor Kaori Tanaka for all the patience with complex calculus and the willingness to help at any time of the day.

I want to give special thanks to my family, who do not understand what I do, but they believe it is important and someone has to do it. To my dad who thinks he will understand some time soon, you wish. To my mom for her caring and supportive love.

I am grateful with all my friends who supported me during these stressful and rewarding period, thanks for all your random questions along the time and those who questioned me if I really wanted to be here. Thanks to Siyuan Li for bringing hugs and clarity to my problems, to Viviana for being the local mom, to Jason Ho for his infinite good will, to Thamirys for all her help using `MATHEMATICA`, to Bernardo and Bardia for all the laughs at the office, to Yohanna who has always believed that my love for physics is bigger than the love I have for her. And all my friends who implicitly were there giving me motivational quotes and who always believed that I could do it: Melisa, Javiera, Alexandra, Aline, Morgana, Leonardo, Fabian, Esteban, William, Patrick, Danae and Marisol.

Special thanks to Francisca (alias Panchi), my twin sister who has always believed in me and encouraged me to pursue this major and had challenged me to do my best every day, even when that would break her heart. To her who always teaches me how to be a better person and who laughs at my nerd jokes without judging. And because she read all the manuscript and she gave her best to understand this topic even when the writer does not even get it. Thanks Panchi, you are my sunshine.

It is fun to speculate about the way **quarks** would behave if they were *physical* particles of finite mass.

- *A schematic model of baryons and mesons*, Murray Gell-mann (1964).

To Panchi.

Contents

List of Tables

List of Figures

List of Abbreviations

SM	Standard Model
LHC	Large Hadron Collider
QCD	Quantum Chromodynamics
QFT	Quantum Field Theory
PT	Perturbation Theory
LHS	Left-hand Side
RHS	Right-hand Side
LO	Leading Order
NLO	Next-to-leading Order
OPE	Operator Product Expansion
VEV	Vacuum Expectation Value
QCDSR	QCD Sum Rules
OPE	Operator Product Expansion

1 Introduction:
On the nature of light exotic hadrons

1.1 Motivation

The desire to explain the universe around us, its evolution and origin, its behaviour and its main constituents has not slowed down with the latest scientific achievements and the confirmation of certain fundamental phenomena; conversely this is opening the door to a promising scientific era where the improvements in technologies and great engineering efforts are allowing us to explore nature beyond the limitations we had in the past.

In the particle physics scene, the hadronic sector (i.e., strongly-interacting particles) has benefited from a substantial progress since the development of collider physics in the 1960's. These experiments have validated, among others, the theory of strong interactions with the confirmation of the existence of hadrons and have revealed some of their most important properties, such as colour confinement and asymptotic freedom [3].

Likewise, the theoretical perspective was also impacted by these experimental results, and in the scope of the strong interactions, the conventional quark model has been subject to some significant extensions that go beyond the initial naive classification of hadrons. As it is understood, the conventional quark model provides a simple categorization of hadrons; mesons as quark-antiquark states and baryons as three quark or three antiquark states. However, physicists had defined a new set of substructures coming from the discovery of new mesons and baryons, where some of the candidates do not follow the simple quark model framework, and based on the underlying theory of this model, Quantum Chromodynamics (QCD), the concept of exotic hadrons with richer quark and gluonic substructures becomes relevant as will be discussed later in Section 1.5 (see e.g., Refs. [1, 2, 4–9] for more reviews on exotic hadrons).

Quantum Chromodynamics (QCD) is a quantum field theory (QFT) that portrays the interaction of quarks and gluons at an elementary level, whose main requirement is to satisfy colour neutrality of hadronic bound states. Hence, the colour-neutrality definition of hadrons as made up of quarks and gluons does not forbid the existence of these exotic states (e.g., glueballs, multiquark states, etc.), leaving the conventional quark model as an incomplete description for this whole new range of states.

Despite the great strides of exotic hadrons studies, the light scalar sector still remains under some uncertainties regarding their structure, including the possibility of quark-antiquark $\bar{q}q$, tetraquark $\bar{q}q\bar{q}q$ and glueball compositions (see e.g., Refs. [1, 10] for a summary on scalar mesons). There exist important questions about how theoretical QCD corrections affect differently the observables of light and heavy systems (see e.g., Refs. [11, 12]).

The controversial and challenging task to identify $q\bar{q}$ states within the low energy sector with quantum numbers $J^{PC} = 0^{++}$ is of our special interest due to their QCD calculation uncertainties in the low-energy regime (see Refs. [13–19] for further details). More specifically, the so-called sigma state σ (or $f_0(500)$) is commonly referred to as one of the most complicated to study, and there are many attempts to understand their structure and obtain unambiguous mass predictions, as manifested in Ref. [1] with a mass range between $400 - 800$ MeV, also see Refs. [11, 20–23] for a deeper overview on this issue.

Given the importance of tetraquark picture for the scalar mesons scheme and the advantages that QCD sum-rules (QCDSR) offer to study these light systems, the main goal of this thesis is to explore these light scalar tetraquark states, study their QCD correlation functions and examine the contribution from the next-to-leading order (NLO) QCD diagrams to the perturbative terms [11] within QCDSR determinations of the light-tetraquark mass predictions.

1.2 Outline

This thesis begins by briefly introducing the baseline theory, the Standard Model (SM) in Sec. 1.3 with the purpose to give the reader an overview of the classification of fields and their role in particle physics. Next, moving deeper into the subject that brings us here, Quantum

Chromodynamics (QCD) in Sec. 1.4, by presenting its features and the definitions of its fundamental fields, i.e., their interactions and mathematical properties in order to understand how the Feynman rules are computed later in Chapter 2. So far, this content is structured to be followed-up by the key aspect of exotic hadrons. Therefore in Secs. 1.5 and 1.5.2, the reader is provided with an introduction to these type of systems, their experimental evidence and the background theory, namely, the ideas beyond the quark model that support the existence of these exotic states.

In Chapter 2 the concept of interpolating currents, QCD correlation function and its counterpart the spectral function are presented thoroughly in order to elaborate the method of QCD sum-rules. The first section of this chapter (Sec. 2.1) gives an insight into the construction of the currents for tetraquark systems with its NLO radiative QCD corrections and their symmetries (e.g., Lorentz invariance and colour symmetry), as well as the associated Feynman diagrams. Later, the goal of Sec. 2.2 is illustrating the relation between the correlation function (also called QCD correlator or simply correlator) and the hadronic spectral function (or spectral density), so as to make the connection between the theoretical calculations at the elementary level and the hadronic properties depicted in experiment. Finally, this chapter concludes with Sec. 2.3, whose objective is to formulate the QCD sum-rules (QCDSR), for instance, Laplace sum-rules, to relate the predictions of this method with the mass estimates.

Chapter 3 outlines the results obtained after a deep analysis of the contribution from the NLO diagrams to the spectral function of the σ state and its effect on the Laplace sum-rules. This chapter starts by exploring the relative weight of the NLO calculations with respect to other main contributions on the spectral function and sum-rule in Sec. 3.1, which will finally translate into a search for a suitable and physical Borel window (τ) for analysis. Later, in Sec. 3.2 through the use of different criteria, a scan on the parameter space of the Borel window and an optimization on the continuum threshold are executed, where lower and upper bounds of τ are to be determined, while the search for the optimal value of the continuum threshold is made through the implementation of two models and their optimization. Finally, after obtaining the QCDSR parameters, a mass prediction is made and then, this result is discussed in Sec. 3.3, whose intention is summarizing the most important results and their

physical meaning.

Finally, Chapter 4 wraps up all the work presented, where the most important conclusions are shown, as well as the future possible ideas to improve and extend the results and the methodology with the key aspects included from the analysis.

Additionally, Appendices A-C have been added in order to complement certain topics in a more comprehensive way, with one section specially devoted to show the preliminary work and analysis of the spectral function of other currents, where a comparison between two methods was made.

1.3 Standard Model

The Standard Model of particle physics (SM) is one of the most accepted and successful theories of fundamental physics (see e.g., Refs. [24–27]). This theory has been demonstrated experimentally throughout the years since the beginning of the 20th century and it was completed in 2012 with the discovery of the Higgs Boson by CERN at the Large Hadron Collider (LHC) [28, 29], which was the missing piece of the theory for many years (see also Ref. [30] for a better understanding of this bosonic field and its exhaustive and historical search).

To begin with, the SM of particle physics is a quantum field theory (QFT) built on three main elements [24]; field theory, special relativity and quantum mechanics. Its construction is based on principles of symmetry, whose algebra is given by group theory. Its constituent objects and the essential structure of the model is founded on the quantum-mechanical global classification of fields as bosons and fermions. Bosons are defined as the integer-spin objects that satisfy the Bose-Einstein statistics, i.e., they follow the commutator field algebra. Within the framework of particle physics, these are commonly said to be the force carriers, meaning that they are responsible for the interactions between all the fields in the model. Fermions are half-integer-spin objects which obey the Fermi-Dirac statistics, satisfying the anticommutator field algebra [24]. These are known as the matter constituents and in terms of the SM theory, they can be subdivided into two sub-categories: leptons and quarks. Let us remark that whilst both leptons and quarks interact through the electroweak interaction involving photons and

massive gauge bosons W and Z, quarks additionally interact through the strong interaction mediated by the massless gauge boson, gluon g, this being a special feature of this sector of the model.

To complete the introduction of the fields of the theory, the last but not least important, the Higgs boson is a particular case of bosons. The Higgs boson is a massive spin-zero particle, whose role through the Higgs mechanism is to give mass to most of the massive fields of the theory (except for possibly the neutrinos), see [24, 25, 31, 32] for more details about the Higgs mechanism.

Now after this introduction that briefly described the fields contained in the SM, attention can be turned to its mathematical structure and its particle content shown in Eq. (1.1) and Fig. 1.1, respectively. The Lagrangian $\mathcal{L}_{SM}$ can be represented as three main sectors:

$$\mathcal{L}_{\mathrm{SM}} = \mathcal{L}_{\mathrm{EW}} + \mathcal{L}_{\mathrm{QCD}} + \mathcal{L}_{\mathrm{H}}, \tag{1.1}$$

where EW is related to the electroweak interactions: these are photons, fermions and massive gauge bosons (W and Z), where the electromagnetic interaction emerges naturally from the electroweak interaction through the $U(1)$ hypercharge. Next piece is the QCD sector, the Quantum Chromodynamics theory regarding the strong interactions, i.e., this includes exclusively quarks (q), antiquarks ($\bar{q}$) and gluons g; and finally the Higgs sector H, which are the terms for the Higgs boson interaction plus the Yukawa terms, being the ones generating the masses.

Fig. 1.1 displays the elementary fields proposed by the SM theory, where blue boxes represent quarks, the orange boxes are the neutral leptons, the red ones are the electrically charged leptons, the yellow boxes are the gauge bosons and finally the Higgs boson is shown in gray on the right-hand-side (RHS). Their properties such as their masses, charges and spin are given by the Particle Data Group in Ref. [1].

Even though the SM provides the basics of particle physics, their interactions and symmetries, this framework does not totally limit the wide range of possible structures composed by these elementary fields; in which case their properties will be ruled by global symmetries imposed by the model, but whose composition can be diverse, for instance being familiar

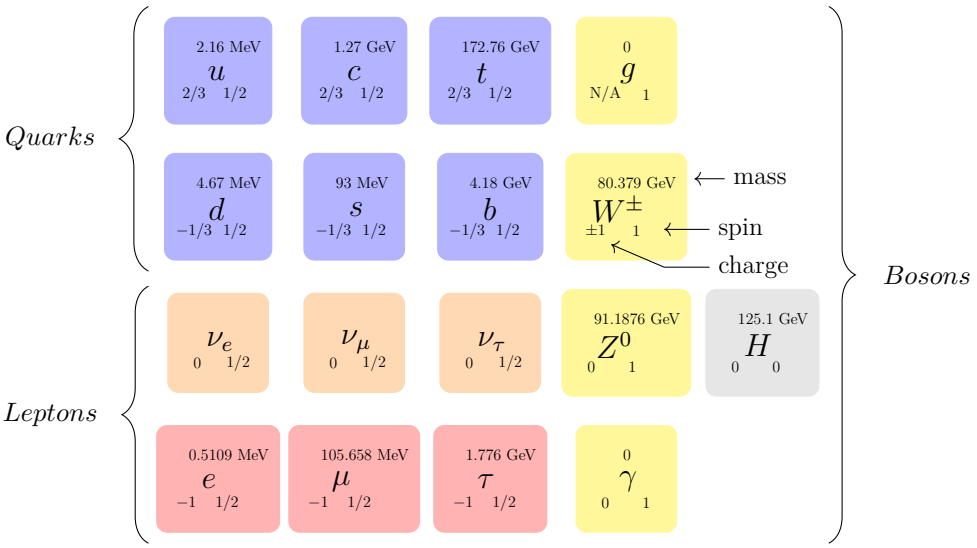

Figure 1.1: Particle content of SM of particle physics and their intrinsic properties: masses, spin and electric charge [1]. The units are considered in the framework of the natural units, i.e., $\hbar = c = 1$, hence the masses are expressed in terms of energy units GeV, as well as the electric charge is expressed in units of fundamental charge e.

examples protons and neutrons.

This important attribute not only allows extensions of the theory, but also the extension of its mathematical applications. This provides a key aspect to study exotic hadrons within the strong interaction sector, QCD.

1.4 Quantum Chromodynamics (QCD)

As mentioned before, this study is mainly focused on Quantum Chromodynamics (QCD) as one special piece of the SM theory. This is a non-Abelian gauge field theory that describes the interactions of the elementary fields: quarks (q), antiquarks ($\bar{q}$) and gluons (g), and particularly how they bind together forming hadrons. Its mathematical structure is ruled by the properties of the colour gauge symmetry group $SU(3)_C$, wherein the fundamental particles q, $\bar{q}$ and the gauge boson g combine to be the hadronic constituents through the strong interaction (see e.g., Refs. [1, 3, 24, 33–36] for a detailed overview of QCD).

Within QCD, it is possible to identify six quark flavours known as up (u), down (d), strange (s), charm (c), bottom (b), top (t) (see Table 1.1 and Fig. 1.1 for masses and electric charge). In addition there are eight massless gauge bosons known as gluons. Quarks are

said to be the fundamental (three-dimensional) representation of the group SU(3), while gluons are described by the adjoint (eight-dimensional) representation [1, 34]. One of the most important features of this theory is the so-called colour as quantum number, hence as an extra degree of freedom. Moreover, along with the fields and their intrinsic quantum numbers, another fundamental parameter to have in mind in QCD is the strong coupling g_s, which represents the strength of the coupling between q, $\bar{q}$ and g.

Flavour	Mass (GeV)	Electric Charge (e)
up (u)	0.00216	+2/3
down (d)	0.00467	-1/3
charm (c)	1.27	+2/3
strange (s)	0.093	-1/3
top (t)	172.76	+2/3
bottom (b)	4.18	-1/3

Table 1.1: Properties of quarks.

The ideas of QCD and colour as a quantum number were first introduced by Oscar W. Greenberg [37, 38], and arose from the need to explain the existence of hadrons. Hadrons were originally understood in the conventional quark model as the simplest colour singlet combinations between q and $\bar{q}$, whose wave function must satisfy the Fermi-Dirac statistics of a total antisymmetric wave function, and this colour feature emerges as a consequence.

In order to see the algebraic structure of the strong interactions theory, the non-quantized QCD Lagrangian piece from Eq. (1.1) is given by:

$$\mathcal{L}_{\text{QCD}} = \bar{\psi}_j^a \left(i\gamma^\mu \left(\partial_\mu \, \delta^{ab} + i g_s \, t_A^{ab} \mathcal{A}_\mu^A\right) - m_j \, \delta^{ab} \right) \psi_j^b - \frac{1}{4} G_{\mu\nu}^A G_A^{\mu\nu}, \tag{1.2}$$

where repeated indices are summed over (see Appendix A for conventions); a, b are the colour indices and run from 1 to 3 (number of colours); ψ_j^a ($\bar{\psi}_j^a$) are the quark (antiquark) fields of flavour j that runs from 1 to 6; $\mathcal{A}_\mu^A$ are the eight gluon fields in the adjoint representation; t_A^{ab} are the matrix representation of the generators of the group $SU(3)$, which satisfies the relation $t_{ab}^A = \frac{1}{2}\lambda_{ab}^A$, λ^A being the Gell-Mann matrices. Ultimately, $G_{\mu\nu}^A$ is the gluon field strength tensor defined as

$$G_{\mu\nu}^A = \partial_\mu \mathcal{A}_\nu^A - \partial_\nu \mathcal{A}_\mu^A + g_s f_{ABC} \mathcal{A}_\mu^B \mathcal{A}_\nu^C, \tag{1.3}$$

where f_{ABC} are the structure constants of the $SU(3)_C$ group and $A,\ B,\ C$ run from 1 to 8. Equations (1.2) and (1.3) show an interesting peculiarity in the gauge-boson sector, where gluons are self-interacting and there are explicit three- and four-gluon interaction vertices, which does not happen in the electromagnetic sector of the theory (SM).

In the scope of this study, the Lagrangian in Eq. (1.2) provides the tool to extract the Feynman rules for quark and gluon interactions, allowing the calculation of observables such as hadronic masses and decay widths by means of perturbative series expansion of the strong-coupling constant $\alpha_s = g_s^2/4\pi$ (α_s for brevity). See Refs. [3, 25, 27, 33] for the full set of Feynman rules and the path to their construction from QFT.

During the early stage of hadronic physics, there were some attempts to explain the idea of hadrons and strong interactions (see e.g., Refs. [39–41] for more details about alternative models), but after a heated debate, the concept of hadrons was finally defined within the conventional quark model scheme. In this context, the QCD theory is one of the tremendous achievements since the quark model was proposed, whose essential role lies on setting the basic rules for the interacting fields composing the hadrons.

1.4.1 Quark model

In 1964, two particle physicists came up independently with the so-called quark model (George Zweig [35] and Murray Gell-Mann [42]) as a way to explain meson and baryon configurations. The proposed ideas were that the hadrons were bound states made up of subatomic elementary particles with fractional electric charge, which were initially called *aces*, but then this name was changed by Gell-Mann to *quarks*. By the time this theory was starting to gain followers, the experimental sector was already showing the discoveries of several hadronic states, such as pions (π), kaons (K), among others, and therefore motivating the theory (see also Ref. [43] for an introduction to the quark model).

Quarks and gluons have never been seen as free particles in experiment and so they are not directly measured, but instead their counterparts are detected, the wide range of hadrons. In this sense, quarks and gluons are seen indirectly as substructure of hadrons. This issue triggered the development of the primitive quark model as a suitable theory by setting a classification scheme for this extensive spectrum of hadrons. Originally, this classification

was formulated spanning the simplest hadronic structures, such as mesons as a pair $q\bar{q}$ and baryons as a group of qqq or $\bar{q}\bar{q}\bar{q}$. Overall, both systems must satisfy one common requirement of colour neutrality, i.e., the total wave function of the hadron must be invariant under $SU(3)_C$ transformations. In other words, it must behave as a singlet under colour transformations.

In spite of the idea that the quark model's attempt to explain the simplest hadrons prevailed for many years and was then validated with the improvements in collider physics, ab-initio Zweig-Gell-Mann [35, 42] model of hadrons did not limit these states to be strictly the simplest compound systems, but rather these bound states must be constrained by the requirement of colour neutrality, leaving the door open for extensions to the broad hadron spectrum, including more complex structures such as four-quark states, pentaquarks, etc. (see also Ref. [44]). Likewise, this colour-neutrality approach was extended to other combinations including the gauge bosons, gluons (e.g., hybrids, glueballs), due to their property of carrying colour charge and its self-interaction shown in the strength tensor field of Eq. (1.3). Henceforth, these combinations beyond the conventional quark model will be referred as exotic hadrons.

1.5 Exotic Hadrons

The incomplete notion that the conventional quark model restricted the classification of hadrons into only irreducible states such as $q\bar{q}$ mesons and qqq or $\bar{q}\bar{q}\bar{q}$ baryons unleashed the urge to add exotic members to the hadron spectrum. The rise of this idea settled strongly among the scientific community, and subsequently throughout the years and with better technologies for hadron spectroscopy, this field has been intensely studied.

To date, exotic hadrons have been consistently searched for in many experiments, whose outstanding progress has yielded remarkable improvements in the theoretical understanding of these exotic states. As a consequence the hadronic physics sector has witnessed the extension of the quark model and the evidence of exotic state candidates [2]. We now have some insights on the possible classification of these exotic states: glueballs as made up purely of gluons, hybrids as a mixture of gluons and quarks/antiquarks, and multiquark states composed by more than three quarks or/and antiquarks.

The big breakthrough came in 2003 with the discovery of the exotic meson $X(3872)$ [1] in the Belle detector at the KEKB[2] collider in Japan [45]. The features of this state showed a composition of at least a charm-anticharm ($c\bar{c}$) pair, but its quantum properties did not fit into an ordinary $c\bar{c}$ quarkonium scenario, suggesting an exotic $c\bar{c}q\bar{q}$ structure. This event marked the beginning of a new era in hadron spectroscopy and revived the interest in studying the exotic sector. For instance, the so-called XYZ resonances stand out among the great variety of states due to the large amount of candidates observed, and year by year this long list increases. These structures are considered to be charmonium-like ($c\bar{c}$-like) states, because of the presence of charm-anticharm pair in its composition as evidenced by J/Φ in decay products, such as the states presented in Fig. 1.2 from Ref. [2].

More information about some of these XYZ states can be found in Refs. [45–57], among other sources. In addition, their cousins are also present in the searches. These are the bottomonium-like ($b\bar{b}$-like) states: as their name indicates, they are composed of at least one bottom-antibottom pair (see Refs. [2,5,58–62] for a detailed analysis of these and other exotic states).

One of the most important states observed is the tetraquark candidate $Z_c^{\pm}(3900)$ (see Refs. [63, 64]), which clearly stands out from the conventional classification of mesons given its electric charge which implies additional quark content beyond $c\bar{c}$, and its composition is suspected to be $c\bar{c}u\bar{d}/c\bar{c}d\bar{u}$. Along with this state, the recently discovered T_{cc}^{+} candidate [65,66] at the LHCb experiment at CERN, presented during the European Physical Society conference on high energy physics (EPS-HEP Conference 2021), is a long-lived exotic tetraquark candidate, whose quark composition is $cc\bar{u}\bar{d}$.

Thanks to all the progress and the evidence provided, there is a clear suggestion manifested that multiquark states exist. For this reason this work is oriented to the study of a specific classification of four-quark states. Among all the exotic states, these are of our special interest and they can be studied from the QCD Sum-rules (QCDSR) approach.

[1] In the Particle Data Group classification scheme, the $X(3872)$ corresponds to a meson of mass 3872 MeV.
[2] $e^{-}e^{+}$ collider.

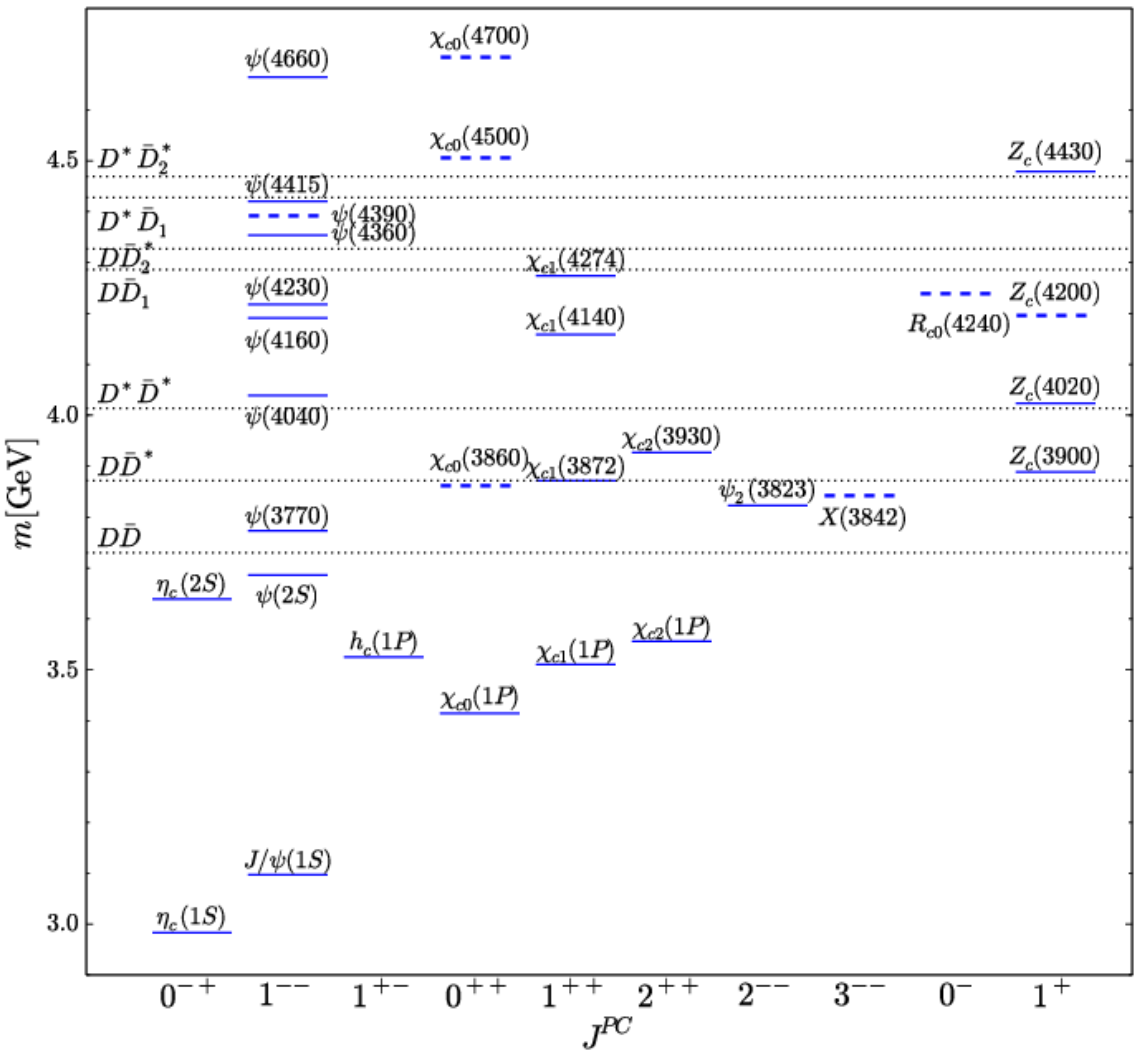

Figure 1.2: Spectrum of states in charmonium ($c\bar{c}$) sector. The solid blue lines represent the states that have been experimentally determined, and the dashed blue lines represent the states that are not established yet by PDG, but they are claimed already as candidates. Image credit N. Brambilla, et al. [2].

1.5.1 Four-quark states

Among the variety of configurations of exotic hadrons, four-quark states are systems composed of four quarks/antiquarks, e.g., $qq\bar{q}\bar{q}$, $q\bar{q}q\bar{q}$, $qq\bar{Q}\bar{Q}$, etc., where q ($\bar{q}$) and Q ($\bar{Q}$) are light and heavy quarks (antiquarks) respectively. These could be subdivided into two types depending on their internal colour substructure: tetraquarks and molecular states (see Fig. 1.3). Tetraquarks are $qq\bar{q}\bar{q}$ configurations such that there are two clusters called diquark (qq) and antidiquark ($\bar{q}\bar{q}$), where each cluster has a certain colour number and altogether form a colour-neutral system. Molecular states are $q\bar{q}q\bar{q}$ configurations, with meson-meson ($q\bar{q} - q\bar{q}$) structures that must satisfy the condition of colour neutrality, with each of these mesons being colour-neutral.

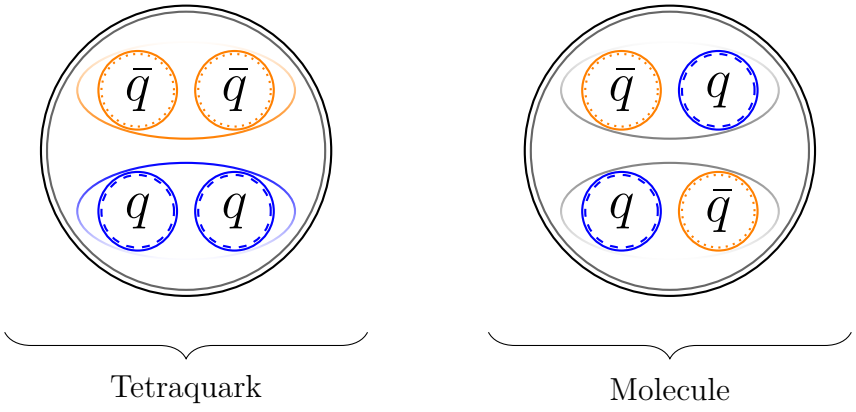

Figure 1.3: Four-quark configurations.

The XYZ tetraquark states previously mentioned are considered within the series of charmonium-like (and additionally with bottomonium-like) are collectively named as heavy tetraquarks. In the framework of QCDSR, the vast majority of QCD sum-rule studies of charmonium- and bottomonium-like tetraquarks have been performed at leading order (LO) in perturbation theory (PT) [58, 67–70]. There are approximate calculations that provide indications that higher-loop effects may be small in the heavy tetraquarks systems [12,71,72]. In contrast, in the light scalar sector there is evidence that these higher-loop contributions may be large in light tetraquark systems (see e.g., Refs. [11, 14]).

1.5.2 Light Scalar Mesons

To date there is still debate on the light scalar sector of QCD. The uncertainties on the knowledge of light hadrons come from poor understanding of QCD at low energies and the experimental complexities of detecting scalars because they have the same quantum numbers as the vacuum. Direct application of QCD at low energies becomes challenging because of the inclusion of the fundamental parameter α_s in the calculations, which behaves according to the energy scale. In the ground state, perturbation theory (PT) can be used partially, given that there are other contributions (QCD condensates) inherent from the hadronic vacuum that must be included.

Naturally, the question of why we want to study the light scalar sector arises. To address this issue we might understand the mesonic picture in terms of quark model predictions, whose results in comparison with the experiment were in agreement for a large range of mesons. That is, except for the light scalar mesons, which seem to be anomalously light [13], and somehow the amount of these states exceeds the number expected in the quark model, including the possibility of a glueball, and so they remain puzzling (see also Refs. [15, 19, 21, 73, 74] for an overview on these mesons and their masses). The aim of studying the light scalar sector and the hunt for glueballs is tightly related to the desire of understanding strong interactions in the low-energy regime, and if possible, get some insights on the chiral symmetry breaking issue, as well as some understanding of colour confinement.

The light resonances are cumbersome to study and detect in the experiment, since it is difficult to measure their signal due to the low-energy background, and their large estimated decay width. When referring to light scalar resonances, these are the ones expected to be in the energy range below 2 GeV. They are said to contain a $qq\bar{q}\bar{q}$ nonet of light scalar states as shown in Fig. 1.4. This idea of light scalar four-quark nonet was developed and presented by Robert L. Jaffe in 1977 [75] (see Ref. [17] for a summary on this nonet), whose classification of the light scalar mesons was elaborated based on the bag model scheme.

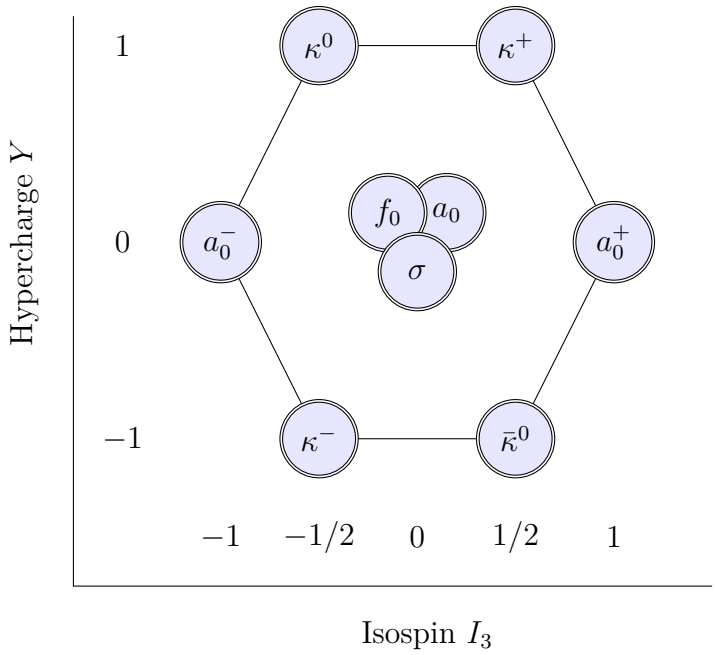

Figure 1.4: Weight diagram of nonet of lightest scalar mesons with their hypercharge (Y) and third component of Isospin (I_3) numbers, where the superindices $(0, +, -)$ indicate the electric charge of the hadron.

Regarding the quark content, the states in Fig. 1.4 are proposed to be composed of $u\,(\bar{u})$, $d\,(\bar{d})$ and $s\,(\bar{s})$ quarks (antiquarks) (see Appendix A for an explicit description of these states) and the combination of them will determine their exotic quantum numbers ($J^{PC} = 0^{++}$ in this case for the σ state) as well as their total hypercharge (Y) and third-component of the isospin (I_3). These systems are understood as a superposition of states, i.e., a mix of the conventional $q\bar{q}$ mesons and the $qq\bar{q}\bar{q}$ tetraquarks states, where there is a strong belief that they have a significant tetraquark component as stated in Ref. [75], see also Refs. [10,13,76–79] for a detailed discussion on the nature of these states.

In order to study observables one must understand the concept of resonances and masses in hadronic physics. On one side, the resonances are somewhat "intermediate" states with a large decay width (short lifetime). Experimentally these resonances are found as narrow peaks in mass or energy distribution plots, and they are characterized by mechanisms such as

$$A + B \quad \rightarrow \underbrace{\mathrm{X}}_{\text{Resonance}} \rightarrow \quad C + D + \ldots, \tag{1.4}$$

where A, B are the initial states with certain properties, and $C, D, \ldots$ are the final states.

On the other hand, quark masses are not directly measured, but rather their influence in hadronic properties and other QCD predictions. Particularly, the quark masses depend on the renormalization scale parameter μ^2 [1] (most commonly named $\mu^2_{\overline{MS}}$ in the $\overline{MS}$ scheme), meaning that the QCD dynamics within hadrons depend on the energy scale, but not the hadron masses themselves. Now, the question is: how do we estimate exotic hadron masses? The mass and width of a certain resonance is given by the nearest pole of the process amplitude (S-matrix) to the energy threshold for the production process. Hence, the formula to study their masses and widths, involving the pole of the S-matrix amplitude is given by

$$\sqrt{s_{\rm pole}} = m_{\rm H} - i\Gamma/2,$$

where $m_{\rm H}$ is the hadronic mass estimate, Γ is the corresponding decay width and $\sqrt{s_{\rm pole}}$ represents the energy where the pole of the amplitude is located in the complex energy plane. The goal of this research is to localize the position of this pole, for which the QCDSR approach is appropriate, and it will be used within the energy below 2 GeV to study primarily the σ mass estimate.

1.5.3 The scalar σ state

There is one state that has been of wide interest, not only because of its structure and its intrinsic complexity when making predictions which are hampered by the low energy effects, but also because of the insightful understanding that it could lead to if its internal structure and mass are finally unraveled. This state is the so-called σ state or $f_0(500)$ [3] with the vacuum quantum numbers $J^{PC} = 0^{++}$ (see Refs. [14] for an extensive history of this state). It is classified as the lightest scalar tetraquark candidate, whose dominant decay mode is believed to be the $\pi\pi$ channel and whose suggested composition is made of u, $\bar{u}$, d and $\bar{d}$ [20, 80].

For many years, there have been plenty of controversy on to whether this state exists or

[3] In PDG terminology, isospin-zero mesons are denoted as f with spin as subscript, and mass in MeV in parentheses.

not and if it does it is whether a conventional $q\bar{q}$ meson or a $qq\bar{q}\bar{q}$ tetraquark configuration [20, 23, 79, 81, 82], or instead what is the main dominant configuration is. This thesis explores the σ scalar in the tetraquark scenario with its perturbative NLO radiative correction to the QCD sum-rule and its subsequent influence on the mass estimate.

2 Theory and Methodology: Correlator, sum-rules and other "complex" stuff

This chapter shows the key theoretical concepts that will be used to have a better understanding of how the QCD Laplace sum-rule analysis is performed (e.g., fundamental parameters and methodology). Starting from the tetraquark current construction based on certain symmetries, such as flavour, colour and Lorentz; thereafter moving to the definition of the spectral function $\rho(s)$ and its relation with the QCD correlator, all of this in the basis of the Feynman rules and the Operator Product Expansion (OPE). The key final result is the connection between the QCD Laplace sum-rules and the hadronic mass estimate $m^2_{\rm H}$.

2.1 Interpolating currents

In the framework of QCDSR, it is crucial to define the concept of currents in order to compute the current correlation function and later make the proper study of the QCD Laplace sum-rules and the observables [83, 84] (see also Ref. [85]). Basically, it is understood that the quantum states can be probed through currents, being the mathematical objects that have the information of the interacting elementary fields composing the hadrons. The construction of these currents depend on the four-quark state structure chosen, for instance, the tetraquark configuration, i.e., a pair of diquark and antidiquark clusters as shown in Fig. 2.1[1].

The possible independent tetraquark currents for the light scalar mesons are split according to the flavour-symmetric and flavour-antisymmetric classification, and their behaviour under Lorentz transformations and colour symmetry group transformations. To begin with,

[1]All the Feynman diagram figures shown in this report were made using the package Tikz-Feynman [86].

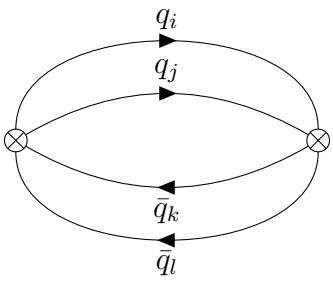

Figure 2.1: Leading-order Feynman diagram of tetraquark configuration, where $q/\bar{q}$ correspond exclusively to light quarks.

the flavour-symmetric interpolating currents are the following (see e.g., Ref. [19] for more details), where $q_{i,j,k,l} = u, d$:

$$\begin{aligned}
J_{S_6} &= (u^{iT} C\gamma_5 d^j)(\bar{u}_i \gamma_5 C\bar{d}_j^T + \bar{u}_j \gamma_5 C\bar{d}_i^T), \\
J_{V_6} &= (u^{iT} C\gamma^\mu \gamma_5 d^j)(\bar{u}_i \gamma_\mu \gamma_5 C\bar{d}_j^T + \bar{u}_j \gamma_\mu \gamma_5 C\bar{d}_i^T), \\
J_{T_3} &= (u^{iT} C\sigma^{\mu\nu} d^j)(\bar{u}_i \sigma_{\mu\nu} C\bar{d}_j^T - \bar{u}_j \sigma_{\mu\nu} C\bar{d}_i^T), \\
J_{A_3} &= (u^{iT} C\gamma^\mu d^j)(\bar{u}_i \gamma_\mu C\bar{d}_j^T - \bar{u}_j \gamma_\mu C\bar{d}_i^T), \\
J_{P_6} &= (u^{iT} C d^j)(\bar{u}_i C\bar{d}_j^T + \bar{u}_j C\bar{d}_i^T).
\end{aligned} \tag{2.1}$$

Similarly, the flavour-antisymmetric tetraquark currents are:

$$\begin{aligned}
J_{S_3} &= (u^{iT} C\gamma_5 d^j)(\bar{u}_i \gamma_5 C\bar{d}_j^T - \bar{u}_j \gamma_5 C\bar{d}_i^T), \\
J_{V_3} &= (u^{iT} C\gamma^\mu \gamma_5 d^j)(\bar{u}_i \gamma_\mu \gamma_5 C\bar{d}_j^T - \bar{u}_j \gamma_\mu \gamma_5 C\bar{d}_i^T), \\
J_{T_6} &= (u^{iT} C\sigma^{\mu\nu} d^j)(\bar{u}_i \sigma_{\mu\nu} C\bar{d}_j^T + \bar{u}_j \sigma_{\mu\nu} C\bar{d}_i^T), \\
J_{A_6} &= (u^{iT} C\gamma^\mu d^j)(\bar{u}_i \gamma_\mu C\bar{d}_j^T + \bar{u}_j \gamma_\mu C\bar{d}_i^T), \\
J_{P_3} &= (u^{iT} C d^j)(\bar{u}_i C\bar{d}_j^T - \bar{u}_j C\bar{d}_i^T),
\end{aligned} \tag{2.2}$$

where S, V, T, A, and P stand for scalar, vector, tensor, axial and pseudoscalar substructures, respectively, and the subscripts of these letters correspond to colour degrees of freedom, related to the color representation, either $\bar{\mathbf{3}}_c$ or $\mathbf{6}_c$ for diquarks ($\mathbf{3}_c$ or $\bar{\mathbf{6}}_c$ for anti-diquarks).

In addition, the properties of the Dirac matrices γ^μ are used:

$$C = i\gamma^0\gamma^2, \qquad \{\gamma^\mu, \gamma^5\} = 0, \qquad \sigma^{\mu\nu} = \frac{i}{2}[\gamma^\mu, \gamma^\nu], \qquad [\gamma^\mu, \gamma^\nu] = 2g^{\mu\nu}, \tag{2.3}$$

where C is the charge conjugation operator and $g^{\mu\nu}$ is the metric tensor (see Appendix A for details on conventions used in this thesis).

After a detailed discussion performed by H. Chen, A. Hosaka and S. Zhu in Ref. [74], mixed currents showed reliable LO calculations in the scope of the sum-rules for the low-lying scalar mesons based on the diquark-antidiquark structure. The best choices found to describe the scalar σ state at LO are [19, 74]:

$$\eta_1 = \cos(\theta) J_{A_6^\sigma} + \sin(\theta) J_{V_3^\sigma}, \tag{2.4}$$

$$\eta_2 = \cos(\theta) J_{A_3^\sigma} + \sin(\theta) J_{V_6^\sigma}, \tag{2.5}$$

where $\cot(\theta) = 1/\sqrt{2}$ is the mixing angle.

The fundamental role of this analysis, meaning the task of selecting the best suitable linear combination of scalar currents, yields a proper construction of the spectral function that represents the tetraquark system and thereby ensures the reliability of the sum-rules. At this stage, having defined the currents associated to the leading-order diagram (see Fig. 2.1), the next-to-leading order (NLO) corrections can be added, whose Feynman diagrams are shown in Fig. 2.2.

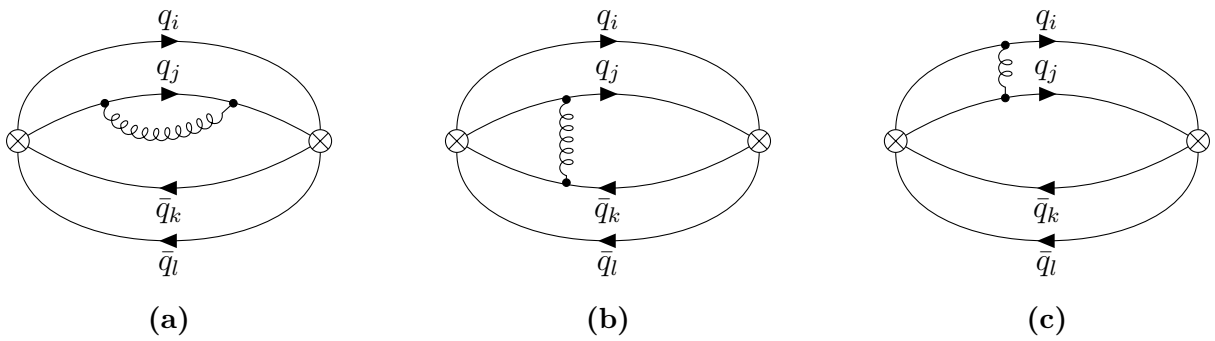

Figure 2.2: NLO Feynman diagrams: (a) self-interaction and (b)-(c) gluon exchange. Notice that other diagrams with similar topologies are omitted in these figures, but used in the calculations.

The essence of these diagrams is to outline the simplest NLO radiative corrections, namely the gluon self-interaction and the gluon exchange between the pairs qq, $q\bar{q}$ and $\bar{q}\bar{q}$, from where the Feynman rules will be constructed using Eq. (1.2). It is noteworthy to mention that the correlation function will contain all the possible diagrams that represent the situation of the gluon exchange, and Fig. 2.2 represents the types of gluon exchange.

2.2 Correlation function and spectral density

Having defined the scalar tetraquark currents in addition with the linear combination required to compute reliable sum-rules, the next step is to formulate the correlation functions and spectral densities.

The underlying goal of the calculation of these functions is to obtain estimates of relevant observables in hadronic physics, such as masses and widths. As a general overview, the current correlator and the spectral function are said to be two representations of the same object [85, 87]. The former is the two-point correlation function $\Pi(x)$ (or two-point Green's function), namely the non-trivial vacuum expectation value (VEV) of the time-ordered product of two local currents, and it is physically understood as the QCD amplitude for propagation of a particle between two spacetime points [33]. On the other hand, the spectral function $\rho(s)$ contains the hadronic properties and thereby the experimental information of the system. Thus the correlation function $\Pi(x)$ represents a theoretical prediction based on quarks and gluons calculations, while the spectral function $\rho(s)$ contains hadronic experimental properties.

To begin with, the current correlation function $\Pi(x)$ is constructed using the definitions of Eqs. (2.4) and (2.5) for the currents, that is

$$\Pi(x) = \langle 0|\mathcal{T}\{J(x)\bar{J}(0)\}|0\rangle = \langle 0|\mathcal{T}\{\eta_a(x)\bar{\eta}_a(0)\}|0\rangle, \tag{2.6}$$

where $a = 1, 2$, $\eta_a(x)$ and $\bar{\eta}_a(0) = \eta_a^\dagger(0)$ (for bosons) are the interpolating currents in coordinate-space (see Eqs. (2.4) and (2.5)), and $\mathcal{T}$ is the time-ordered operator. Moving

to momentum space through the Fourier transform, the correlation function becomes

$$\Pi(q^2) = i \int d^4x \, e^{iq\cdot x} \, \langle 0|\mathcal{T}\{\eta_a(x)\eta_a^\dagger(0)\}|0\rangle. \tag{2.7}$$

In the scope of QCDSR's, the correlation function is related to the spectral density on the basis of the Quark-Hadron duality concept [87–89], i.e., there is a correspondence between theoretical QCD and its phenomenological counterpart [83, 84]. This relation has its foundations on the optical theorem, whose role, by invoking the Cauchy theorem, is to connect the imaginary part of the QCD correlation function with the physics on the real axis of the complex squared energy plane, where the singularities take place [85, 90]. This discontinuity gives rise to the hadronic spectral function, and its poles are understood as the representation of stable hadrons and resonances.

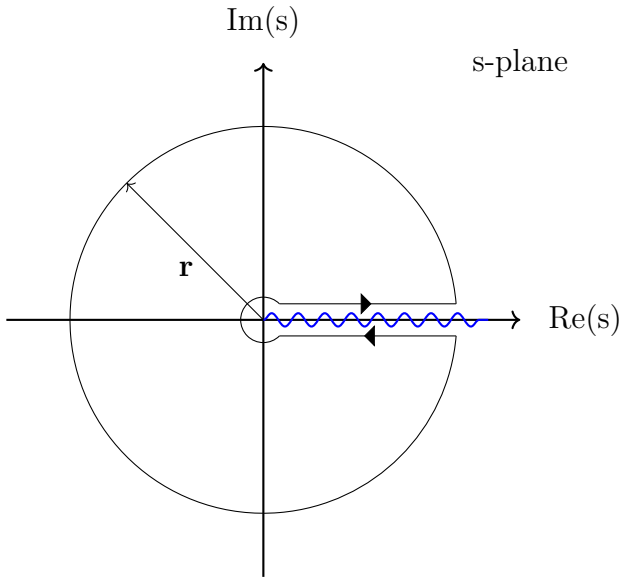

Figure 2.3: Complex squared energy s-plane, where the poles and cuts are located on the real axis, and r is the raduus of the circle, which usually is taken as $r \to \infty$.

From Fig. 2.3, it is possible to study the physics on the real axis by studying the imaginary part of the correlator, where one can separate the integral in the following way [91]:

$$\Pi(q^2) = \frac{1}{2i\pi} \oint_{|s|=r} ds \, \frac{\Pi(s)}{s-q^2} + \frac{1}{2i\pi} \int_{t_0}^{r} ds \, \frac{\Pi(s+i\epsilon) - \Pi(s-i\epsilon)}{s-q^2}. \tag{2.8}$$

Here t_0 corresponds to the physical threshold of the system; in other words, the minimal

energy for the process to occur. The first term in Eq. (2.8) represents the contour integral along the outer circle, while the second term is the one associated to the real axis. This relation is the key aspect to understand duality in hadronic physics.

In order to illustrate this, let us have in mind the idea that Källen and Lehmann established for correlation function representations, where the two-point functions are related with the spectral density [33] through the so-called dispersion relations. Let q^2 be defined as the Minkowskian momentum, which is related to the Euclidean momentum as $Q^2 = -q^2$. The simplest dispersion relation can be written as

$$\Pi^{\rm QCD}(Q^2) = \frac{1}{\pi}\int_{t_0}^{\infty} ds\, \frac{\rho^{\rm had}(s)}{s+Q^2} \; + \; \text{subtraction terms}, \tag{2.9}$$

where $\Pi^{\rm QCD}(Q^2)$ is the QCD correlator, $\rho^{\rm had}(s)$ is known as the hadronic spectral function, and the subtraction terms are related to the divergences coming from the $\Pi^{\rm QCD}$ because of the composite operator aspect of the currents.

Furthermore, QCD requires different treatments in the low- and high-energy regimes. In the low-energy sector, $\Pi^{\rm QCD}(Q^2)$ must contain non-perturbative effects related to the vacuum, which are included via the Operator Product Expansion (OPE), so that the correlator is expressed as an expansion in terms of local operators separated by short distances. Thus, given the definition of $\Pi^{\rm QCD}(Q^2)$ from Eq. (2.6), this new representation will be parametrized as [36]

$$\langle 0|\mathcal{O}_1(x)\mathcal{O}_2(y)|0\rangle = \langle \mathcal{O}_1(x)\mathcal{O}_2(y)\rangle \rightsquigarrow \lim_{x\to y}\sum_n C_n(x-y)\langle \mathcal{O}_n(y)\rangle, \tag{2.10}$$

where $\mathcal{O}_{1,2}(x)$ are composite operators, $\mathcal{O}_n(x)$ are some local operators and $C_n(x)$ are perturbatively calculated Wilson coefficients.

To calculate the vacuum expectation values (VEV's) of a product of operators, the use of OPE is convenient when different vacuum dynamics govern low- and high-energy scale (long- and short-distances). Basically, the OPE is made of perturbation theory (PT) terms and then followed by non-perturbative (non-PT) terms embedded in vacuum expectations values (QCD condensates). This is a special feature of the QCD vacuum and allows the correlation

function to be written in terms of QCD degrees of freedom as well as including the distinctive colour confinement.

To obtain these terms, PT and non-PT, two approaches are taken. The former, PT terms, are calculated using the corresponding Feynman rules from Eq. (1.2), likewise the radiative corrections, the NLO PT terms [11]. Fundamentally, these terms portray the interactions at the elementary level of quarks and gluons, representing QCD theoretical calculations. The latter, non-PT terms correspond to the QCD condensates, whose role is understood to be responsible of the hadronic vacuum properties at low-energy regime, where the strong coupling is large [68,92] and go beyond perturbation theory. The OPE respectively factorizes the low- and high-energy effects into the QCD condensates and into the perturbatively-calculated Wilson coefficients.

In the hadronic sector, it is convenient to work with the hadronic spectral function $\rho^{\text{had}}(s)$ in a similar way, meaning that the low-energy sector will be separated from the high-energy sector in order to study the resonance phenomenology, and mostly decrease the continuum contribution to the spectral function and emphasize the resonances. Thereby, the adoption of the "resonance(s) plus continuum" model is practical, since it allows to study the resonances somewhat isolated from the continuum,

$$\rho^{\text{had}}(s) = \rho^{\text{res}}(t_0 < s < s_0) + \rho^{\text{cont}}(s_0 < s < \infty), \tag{2.11}$$

where t_0 is the physical threshold and s_0 is the continuum threshold. The labels "res" and "cont" refer to resonance and continuum, respectively.

It is important to stress that the study of the lightest states must have appropriate models depicting the possible outcomes. This thesis explores two suitable approaches to examine the resonances from the spectral density, the single narrow resonance and double narrow resonance as outlined below.

Single Narrow Resonance:

This model assumes that the pole of the spectral density corresponds to a single narrow resonance, hence parametrizing the spectral function into two segments with a prominent peak associated with the delta function,

$$\rho^{\text{had}}(s) = \underbrace{f_H \delta(s - m_H^2)}_{\text{Narrow Resonance}} + \underbrace{\theta(s - s_0)\frac{1}{\pi}\text{Im}\Pi^{\text{cont}}(s)}_{\text{QCD Continuum}}, \tag{2.12}$$

where f_H is the strength with which the resonance couples to the vacuum through the chosen current, m_H^2 represents the hadronic mass of the resonance under consideration, and the last term of Eq. (2.12) corresponds to the imaginary part of the QCD correlator within the continuum interval of energy, where there are no singularities.

Double Narrow Resonance:

This model considers the presence of a second resonance affecting the spectral function, meaning there could be a mixing between the states, which is possible when the states share the same quantum numbers, in which case the resonance sector of the spectrum will be

$$\rho^{\text{res}}(s) = \sum_i A_i \delta(s - m_i^2). \tag{2.13}$$

For the lightest scalar mesons (σ and $f_0(980)$), this becomes

$$\rho^{\text{res}}(s) = A_\sigma \delta(s - m_\sigma^2) + A_{f_0} \delta(s - m_{f_0}^2), \tag{2.14}$$

where m_σ^2 and $m_{f_0}^2$ are the masses of the lightest resonances that characterize the hadronic spectral function with mixed states; A_σ and A_{f_0} are the resonance strengths of each state into the spectral function.

The next section outlines methods to extract information of the lightest scalar σ, with the inclusion of $f_0(980)$ as the next-heavier scalar state, from the dispersion relations as well as a methodology to separate the lightest contributions from the continuum.

2.3 QCD Laplace sum-rules

Following the ideas introduced in the previous section, QCD sum-rules (QCDSR) is a method proposed by M. A. Shifman, A. I. Vainshtein and V. I. Zakharov (SVZ hereafter, see Refs. [83, 84]) in the late seventies with the initial purpose to compute hadronic properties from QCD calculations, such as magnetic moments or ground-state masses. Later, this successful approach based on approximations and assumptions extended its applications, from where it emerged the idea that QCDSR can provide constraints on integrals of hadronic spectral functions (see e.g., Refs. [83, 84] for QCDSR foundations).

The main idea of this method is to elucidate QCD at low-energy by studying hadronic spectral functions and by emphasizing the low energy states, namely the ground states. For instance, the so-called Laplace sum-rule (also known as Laplace-Borel sum-rule) is used to enhance the dominance of the lightest resonances in the energy spectrum (see Refs. [91, 93] for reviews), whose foundations were built in terms of the Laplace and Borel transforms, which gave it the name.

The importance of this formulation lies in the relation between the Borel transform operator and the inverse Laplace transform by somewhat modifying the correlator in order to get rid of the unknown and divergent subtraction terms and suppress the high-energy contributions of the hadronic spectral function.

2.3.1 Borel Transform

Given that the goal of this study is focused on ground states of light systems, Eq. (2.9) is not suitable for further calculations in the low-energy regime, due to the divergent polynomials (substraction terms) and spectral function contributions at high energy. Hence, rewriting this expression with the purpose of emphasizing the lowest-energy sector is needed. To achieve this, SVZ [83,84] proposed the method to improve the dispersion relations based on the Borel transform operator and its relation to the inverse Laplace transform, with the help of the

N-*th* derivative applied to the correlation function, as follows

$$\hat{B} \equiv \lim_{\mathrm{N},\mathrm{Q}^2\to\infty} \frac{(-Q^2)^N}{\Gamma(N)} \left(\frac{d}{dQ^2}\right)^N, \quad \text{where} \quad \tau \equiv N/Q^2, \tag{2.15}$$

where the so-called Borel parameter is defined as the fixed ratio τ. This operator has the advantage of annihilating the subtraction terms in the dispersion relation in Eq. (2.9), and its properties are the following [94]

$$\hat{B}[a_0 + a_1 Q^2 + \ldots a_m Q^{2m}] = 0, \quad \text{for} \quad m > 0 \ (m \text{ finite}); \tag{2.16}$$

$$\hat{B}\left[\frac{Q^{2n}}{t+Q^2}\right] = \tau(-1)^n t^n \, e^{-t\tau}, \quad \text{for} \quad n > 0. \tag{2.17}$$

The RHS of Eq. (2.17) shows an explicit dependence on the Borel parameter τ, also referred to as the Borel mass $\tau = 1/M_B^2$, whose dimensions are inverse to the squared energy ($[\tau] = \mathrm{GeV}^{-2}$).

The Laplace transform of an analytic function $f(Q^2)$ is given by (see e.g., Refs. [95, 96] for more details about Laplace and Borel transforms),

$$f(Q^2) = \int_0^\infty d\tau \, F(\tau) \, e^{Q^2\tau} \equiv \mathcal{L}[F(\tau)], \tag{2.18}$$

where

$$\mathcal{L}^{-1}\mathcal{L}[F(\tau)] = \mathcal{L}^{-1}[f(Q^2)] = F(\tau). \tag{2.19}$$

Moving to the complex Q^2-plane, the definition of the inverse Laplace transform will be

$$\mathcal{L}^{-1}[f(Q^2)] = \frac{1}{2\pi i} \int_{a-i\infty}^{a+i\infty} dQ^2 \, f(Q^2) \, e^{Q^2\tau}. \tag{2.20}$$

Then, Eq. (2.20), for any function $f(Q^2)$, is related to the Borel transform operator [97] as

$$\frac{1}{\tau}\hat{B}\big[f(Q^2)\big] = F(\tau) = \mathcal{L}^{-1}\big[f(Q^2)\big], \tag{2.21}$$

Now, one can define a function $\mathcal{L}_k(\tau)$ representing this inverse Laplace transform (see Appendix B for more details),

$$\mathcal{L}_k(\tau) = \mathcal{L}^{-1}\Big[(-1)^k Q^{2k}\Pi(Q^2)\Big] = \frac{1}{\pi}\int_{t_0}^{\infty} ds\; s^k e^{-s\tau}\rho^{\text{had}}(s), \quad \text{for } k \geq 0. \tag{2.22}$$

Therefore, the Laplace sum-rule naturally emerges, and its consequence is the improvement of the dispersion relations as follows:

$$\mathcal{L}_k(\tau) \equiv \frac{1}{\pi}\int_{t_0}^{\infty} ds\; s^k e^{-s\tau}\rho^{\text{had}}(s), \quad \text{for } k \geq 0. \tag{2.23}$$

The importance of this method lies in the effects of the exponential $e^{-s\tau}$ in the integral above, due to its ability to enhance low-energy states and suppress excited ones and the continuum. This expression in Eq. (2.23) denotes the Laplace sum-rule. In the next sections, the final formulation related to QCD and resonance hadronic physics will be shown.

2.3.2 Laplace sum-rule

The comparison between the dispersion relation shown in Eq. (2.9) and the one obtained in Eq. (2.23) demonstrates how the use of the Laplace and Borel transforms improve the quality of the information that can be extracted from the spectral density and from QCD calculations. This establishes the importance of the QCD sum-rules application in hadronic physics to study bound states and resonances.

As presented previously, the "resonance(s) plus continuum model" helps the study by separating the energy ranges. In this instance, the continuum term in Eq. (2.23) can be written as [94]

$$c_k(\tau, s_0) = \frac{1}{\pi}\int_{s_0}^{\infty} ds\, s^k\, e^{-s\tau}\, \text{Im}\Pi^{\text{cont}}(s). \tag{2.24}$$

And this expression combined with Eq. (2.23) results in

$$\begin{aligned}\mathcal{R}_k(\tau, s_0) &\equiv \mathcal{L}_k(\tau) - c_k(\tau, s_0) \\ &= \frac{1}{\pi}\int_{t_0}^{\infty} ds\; s^k e^{-s\tau}\rho^{\text{had}}(s) - \frac{1}{\pi}\int_{s_0}^{\infty} ds\, s^k\, e^{-s\tau}\,\text{Im}\Pi^{\text{cont}}(s).\end{aligned} \tag{2.25}$$

Here, the final formulation for the Laplace sum-rule connecting the hadronic properties with the corresponding QCD calculations will be

$$\mathcal{R}_k(\tau, s_0) = \frac{1}{\pi}\int_{t_0}^{s_0} ds\, s^k\, e^{-s\tau}\,\rho^{\text{res}}(s), \quad \text{for } k \geq 0, \tag{2.26}$$

where $\mathcal{R}_k(\tau, s_0)$ is the entity commonly referred to as the sum-rule, t_0 is known as the physical threshold, which will be taken as $t_0 = 0$, since the study is centered in the light quark sector where m_u and m_d are negligible; s_0 is the continuum threshold separating the resonance from the continuum, and τ is the Borel parameter that works as an auxiliary parameter.

2.3.3 Single Narrow Resonance model

When studying quantum states, different approaches can be taken in order to compute observables. In the same way different techniques and models are implemented during the process with the purpose of highlighting certain states. In this regard, the single narrow resonance model defined in Section 2.2, aims to isolate a given resonance from the continuum region of the spectral density, and it will modify the Laplace sum-rule in Eq. (2.26) as

$$\mathcal{R}_k(\tau, s_0) = \frac{1}{\pi}\int_{t_0}^{s_0} ds\, s^k\, e^{-s\tau}\,\rho^{\text{res}}(s) = f_H m_H^{2k}\, e^{-m_H^2\tau}, \tag{2.27}$$

where $k = 0, 1$ are commonly used because higher weights (i.e., $k > 1$) will increase the continuum contribution.

Within this model, it is straightforward to see how the resonance mass m_σ can be extracted through the following ratio

$$-\frac{1}{R_0\tau, s_0)}\frac{dR_0(\tau, s_0)}{d\tau} = m_H^2, \tag{2.28}$$

or in other words, for the σ mass

$$\frac{\mathcal{R}_1(\tau, s_0)}{\mathcal{R}_0(\tau, s_0)} = m_\sigma^2. \tag{2.29}$$

Using this parametrization, the σ mass is expected to be computed, in which case a Borel window for τ is required to be adjusted and an optimization on a fixed value of s_0 is needed.

2.3.4 Double Narrow Resonance model

Following the same previous idea regarding the quantum states, it is not unreasonable to think there can be mixing between them, meaning that states with the same quantum numbers can couple to the current under consideration with different resonance strengths, hence leaving the door open to make the analysis for more than one resonances at low-energy regime (below 2 GeV). In this scenario, the "resonance(s) plus continuum" model is extended by adding another state in the resonance sector of the spectral function, transforming the sum-rule of Eq. (2.26) by replacing Eq. (2.14) into,

$$\mathcal{R}_k(\tau, s_0) = \sum_i A_i m_i^{2k}\, e^{-m_i^2\tau}. \tag{2.30}$$

This equation above is the so-called multiple resonance model. In this thesis, it will be treated for two resonances, the σ and $f_0(980)$ (for brevity, it will be denoted by f_0)

$$\mathcal{R}_k(\tau, s_0) = A_\sigma m_\sigma^{2k}\, e^{-m_\sigma^2\tau} + A_{f_0} m_{f_0}^{2k}\, e^{-m_{f_0}^2\tau}. \tag{2.31}$$

Notice that this representation is valid for $k \geq 0$, and the term m_i^{2k} comes directly from the definition of the sum-rule with the delta function in the parametrized spectral function.

The sum-rule analysis becomes dependent on these two lightest resonances and the σ mass cannot be directly extracted from the ratio in Eq. (2.29), but instead the ratio will be

$$\frac{\mathcal{R}_1(\tau, s_0)}{\mathcal{R}_0(\tau, s_0)} = \frac{A_\sigma m_\sigma^2\, e^{-m_\sigma^2\tau} + A_{f_0} m_{f_0}^2\, e^{-m_{f_0}^2\tau}}{A_\sigma\, e^{-m_\sigma^2\tau} + A_{f_0}\, e^{-m_{f_0}^2\tau}}. \tag{2.32}$$

This model will be explored by calculating the LHS of Eq. (2.32) and by adjusting the

input parameters on the RHS, such as s_0, τ and the properties of the lightest scalar states, the σ and $f_0(980)$, in order to get an estimation for m_σ.

3 Results:
What about the NLO effects?

This chapter presents the main results in terms of the spectral functions of the associated tetraquark currents, as well as an analysis of the QCD Laplace sum-rule using two different strategies including the single narrow resonance analysis, where the σ state is studied isolated in the low-energy regime; and the double narrow resonance analysis. In a double resonance analysis possible mixing of states could be happening, thus considering some influence from the next-lightest scalar resonance to the sum-rules. Later the optimization of the QCDSR parameters with this mixing aspect included is made, and consequently establishes a robust range on the σ mass from NLO PT effects.

3.1 Tetraquark Spectral function

To begin with, the spectral function of the tetraquark states was computed by H. Chen, A. Hosaka and S. Zhu in Ref. [19] using the OPE method, which included the LO PT term plus the non-perturbative contributions, namely, the QCD condensates.

In addition, the radiative corrections to the PT terms (NLO corrections) shown in Fig. 2.2 were added to this spectral function in accordance to the results obtained by S. Groote, J. G. Körner and D. Niinepuu in Ref. [11]. It is important to remark that some of the results presented in Ref. [11] were inconsistent throughout [11]. The necessary modifications were made through correspondence with the author (S. Groote) [98], who acknowledged, identified and clarified this issue and the existing typos, from which the final NLO contribution to the spectral density was obtained and provided in this thesis, and subsequently it allowed a comprehensive study of the NLO effects on the QCDSR analysis.

In Ref. [19], it is shown that there is a pair of mixed currents, labelled as ρ_1^q and ρ_2^q, that

give reliable Laplace sum-rules[1] for the LO terms, and thus these spectral functions can be studied within this approach. The construction of the diagonal spectral functions was made by means of the terms stated in Eqs. (2.4) and (2.5), resulting in the following expression for ρ_1^σ

$$\rho_1^\sigma = \cos^2(\theta)\rho^\sigma_{A_6A_6} + \sin^2(\theta)\rho^\sigma_{V_3V_3} + 2\sin(\theta)\cos(\theta)\rho^\sigma_{A_6V_3}, \tag{3.1}$$

where $\cot(\theta) = 1/\sqrt{2}$ corresponds to the mixing angle [74]. Let us mention that ρ_2^σ plays the same role in the sum-rule, given the negligible difference with ρ_1^σ, where the NLO PT correction term is the same in both cases, and then all the results will be shown only for ρ_1^σ.

Equation (3.1) is constructed using the definitions of each single mixed spectral function NLO PT contribution as computed by [11], which are

$$\rho^\sigma_{A_6A_6}(s) = \frac{8s^4}{15(4\pi)^6}\left\{1 + \frac{\alpha_s}{\pi}\left(\frac{55}{4} + \frac{5}{2}\ln\left(\frac{\mu^2_{\overline{MS}}}{s}\right)\right)\right\}, \tag{3.2}$$

$$\rho^\sigma_{V_3V_3}(s) = \frac{4s^4}{15(4\pi)^6}\left\{1 + \frac{\alpha_s}{\pi}\left(\frac{67}{10} + \ln\left(\frac{\mu^2_{\overline{MS}}}{s}\right)\right)\right\}, \tag{3.3}$$

$$\rho^\sigma_{A_6V_3}(s) = -\frac{4s^4}{5(4\pi)^6}\left\{\frac{\alpha_s}{\pi}\left(\frac{16}{5} + \ln\left(\frac{\mu^2_{\overline{MS}}}{s}\right)\right)\right\}, \tag{3.4}$$

where Eq. (3.4) corresponds to the corrected terms from the original work in [11, 98]. Therefore, substituting Eqs. (3.2), (3.3) and (3.4) into Eq. (3.1), the PT terms up to NLO will be

$$\rho_1^\sigma(s) = \frac{s^4}{11520\pi^6} + \frac{s^4}{11520\pi^6}\left(\frac{\alpha_s}{\pi}\left[\frac{(409 - 192\sqrt{2})}{40} + \frac{(7 - 6\sqrt{2})}{4}\ln\Big(\frac{\mu^2_{\overline{MS}}}{s}\Big)\right]\right). \tag{3.5}$$

Equation (3.5) represents the corrected and updated spectral function from Ref. [11] based on the correspondence with the author [98].

The very first term in Eq. (3.5) is describing the LO PT term, whereas the following terms correspond to the NLO PT contributions coming from the diagrams in Fig. 2.2. The goal here is to examine the impact of the NLO PT terms on the spectral function and then

[1] Meaning the spectral functions are positive across the necessary energy range.

compare the relative weight of these NLO terms with respect to the LO PT terms within the full QCDSR.

The total NLO spectral function for the σ scalar containing all the terms, PT and non-PT is shown below [11, 19]. From now on, $\rho_1^\sigma(s)$ will be denoted as $\rho(s)$ for simplicity.

$$\begin{aligned}\rho(s) =& \frac{1}{11520\pi^6}s^4\left(1+\frac{\alpha_s}{\pi}\left[\frac{409-192\sqrt{2}}{40}+\frac{7-6\sqrt{2}}{4}\log\Big(\frac{\mu^2_{\overline{MS}}}{s}\Big)\right]\right)\\ &-\frac{m_u^2+m_d^2}{288\pi^6}s^3+\left(4\pi\frac{6\sqrt{2}+7}{9216\pi^6}\langle\alpha_s GG\rangle+\frac{(m_u+m_d)\langle\bar{q}q\rangle}{36\pi^4}\right)s^2\\ &+\left(-4\pi\frac{6\sqrt{2}+7}{1536\pi^6}(m_u^2+m_d^2)\langle\alpha_s GG\rangle+4\pi\frac{m_u m_d\langle\alpha_s GG\rangle}{512\pi^2}\right.\\ &\left.-\frac{(m_u^3+4m_u^2m_d+4m_um_d^2+m_d^3)\langle\bar{q}q\rangle}{6\pi^4}\right)s+\frac{(5m_u^2+20m_um_d+5m_d^2\langle\bar{q}q\rangle^2)}{9\pi^2}\\ &+4\pi\frac{6\sqrt{2}+1}{1152\pi^4}(m_u+m_d)\langle\alpha_s GG\rangle\langle\bar{q}q\rangle-\frac{(m_u^2m_d+m_um_d^2)\langle\bar{q}\sigma Gq\rangle}{6\pi^4},\end{aligned} \tag{3.6}$$

where each term in this equation plays a part in the OPE expansion, and the dimensional consistency is achieved with the polynomial coefficients such as the QCD condensates and mass terms, which compensate the mass dimensions. The OPE terms (i.e., the operators) are ordered in increasing mass dimensions, where PT terms correspond to dimension zero, and so the next terms are the following: $\langle q\bar{q}\rangle$ (dimension 3), $\langle\alpha_s GG\rangle$ (dimension 4), $\langle\bar{q}q\rangle^2$ (dimension 6), $\langle\alpha_s GG\rangle\langle\bar{q}q\rangle$ (dimension 7), $\langle\bar{q}\sigma Gq\rangle$ (dimension 8).

3.1.1 QCD input parameters

The QCDSR analysis will be performed using the updated values of the known condensates and the QCD parameters, from Refs. [74, 91, 92, 99]

$$\langle\bar{q}q\rangle=-(0.240)^3\ \text{GeV}^3, \tag{3.7}$$

$$\langle\alpha_s GG\rangle=0.075\ \text{GeV}^4, \tag{3.8}$$

$$\langle m\bar{q}q\rangle=-\frac{1}{2}f_\pi^2m_\pi^2=-8.281\times10^{-5}\ \text{GeV}^4, \tag{3.9}$$

$$\langle g^2\bar{q}\sigma Gq\rangle=-M_0^2\times\langle\bar{q}q\rangle,\quad M_0^2=(0.8\pm0.2)\ \text{GeV}^2. \tag{3.10}$$

Additionally, the one-loop running coupling α_s is defined as a function of the renormalization scale $\mu^2_{\overline{MS}}$ [92, 100],

$$\alpha_s(\mu^2_{\overline{MS}}) = \frac{\alpha_\tau}{1 + \frac{25}{12\pi}\alpha_\tau \log\left(\frac{\mu^2_{\overline{MS}}}{m^2_\tau}\right)}, \tag{3.11}$$

and from [1]

$$\alpha_\tau = \alpha_s(m^2_\tau) = 0.325 \pm 0.016,$$

where α_τ is a reference value of the running coupling at the energy scale of the τ lepton mass, $m_\tau = 1.776 \pm 0.0012$ GeV [1], and $\mu^2_{\overline{MS}}$ is the renormalization scale parameter in the modified minimal subtraction scheme.

Having all the fundamental parameters defined, the spectral density contributions were computed separately and they are displayed in Fig. 3.1, where each curve represents the contribution by mass dimension of the operators in the OPE. From Fig. 3.1 it is evident that the main contribution comes from the non-perturbative dimension 4 term of the OPE expansion, which corresponds to the gluon condensate $\langle \alpha_s GG \rangle$.

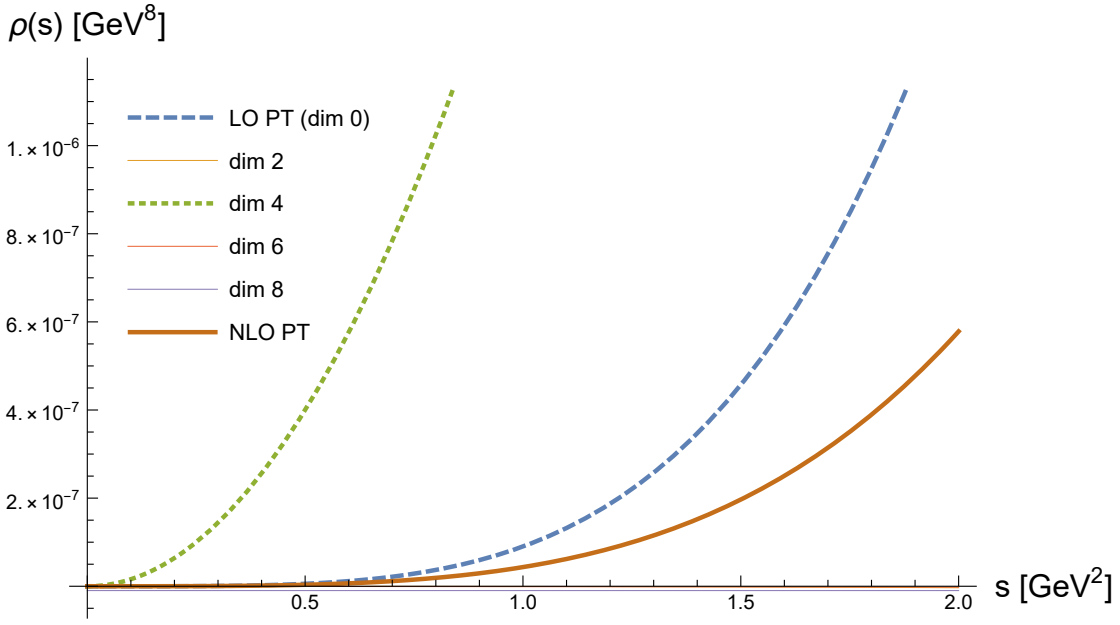

Figure 3.1: Relative contributions to the spectral density $\rho(s)$ by powers of OPE mass dimensions.

Then, the total spectral functions with all the PT and non-PT terms are shown in Fig.3.2, where the comparison between the LO calculations and NLO is displayed.

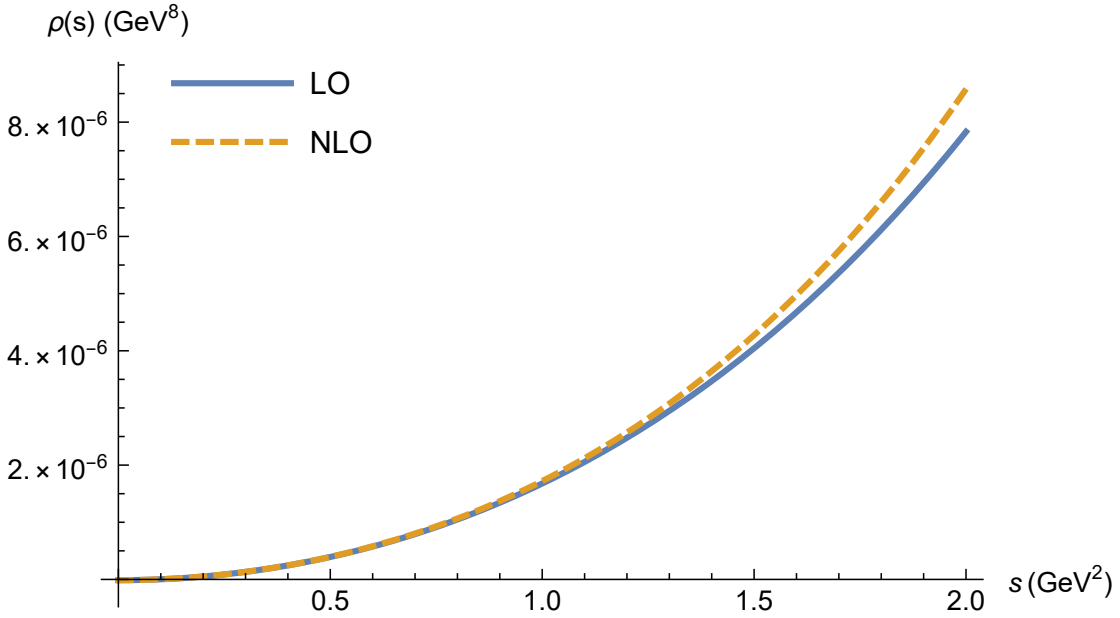

Figure 3.2: Spectral density $\rho(s)$ for LO and NLO results vs energy scale s including all the contributions.

These curves show an approximate similar behaviour, but why? The explanation comes from the gluon condensate term $\langle\alpha_s GG\rangle$, whose weight dominates the spectral function at this energy scale, but leaves room to see the effects of the NLO PT on the total function. For instance, the spectral function of Eq. (3.6) at $s = 1$ GeV^2 can be calculated in order to see the contribution from each term:

$$\begin{aligned}\rho\,(s = 1\,\text{GeV}^2) = \Big[&9.03 \times 10^{-8}(\text{LO PT}) + 4.35 \times 10^{-8}(\text{NLO PT}) \\ &- 4.21 \times 10^{-10}([d]^2) + (1.65 \times 10^{-6} - 4.72 \times 10^{-8})([d]^4) \\ &+ (-1.15 \times 10^{-9} + 9.54 \times 10^{-11} + 9.25 \times 10^{-11})([d]^6) \\ &+ (3.39 \times 10^{-9} - 1.32 \times 10^{-8} - 1.39 \times 10^{-11})([d]^8)\Big]\,\text{GeV}^8,\end{aligned} \tag{3.12}$$

where $[d]^n$ corresponds to the mass dimension of the operators in the OPE.

As expected, the contributions from the LO PT, NLO PT terms and the ones proportional to the dimension 4 condensate in Fig. 3.1 stand out from the other terms, showing their strength in the total spectral function. The 'dim 4' ($[d]^4$) term from Eq. (3.12) is dominated

by the gluon condensate $\langle \alpha_s GG \rangle$, whose prominent weight is commonly associated to hadronic properties in the vacuum, but which contribution becomes less important at higher energy.

A simple way to observe the relative importance of the NLO PT with respect to the LO PT term, is by taking the ratio of the spectral function portions containing these two terms, with the purpose to expose the magnitude of the NLO effects on $\rho(s)$. Even though Eq. (3.12) partially shows this feature, checking its effects in a larger energy region helps with the interpretation.

Energy (GeV^2)	$\rho^{\text{PT}}_{NLO}/\rho^{\text{PT}}_{LO}$ terms
$s = 0.3$	74.2%
$s = 0.7$	53.7%
$s = 1.0$	48.1%
$s = 1.2$	45.7%
$s = 1.5$	43%
$s = 2.0$	40%

Table 3.1: Ratio of NLO PT term with respect to LO PT term in the spectral function at different energy scales.

Across the energy range of Table 3.1, the NLO effects on the spectral function are non negligible, and foremost supports the idea that these NLO diagrams add important corrections to the spectral function. Despite the difference between the first and last terms in the table ($s = 0.3$ GeV^2 and $s = 2$ GeV^2, respectively), the weight in both cases is sufficiently large that the NLO PT terms does not pass unnoticed and must be considered in QCD theoretical calculations.

Wrapping up this section, it was shown that NLO PT contributions to the hadronic spectral function are numerically important in the energy range under investigation.

3.2 QCD Laplace Sum-Rules

As presented previously, there are large contributions from NLO PT corrections to the spectral function $\rho(s)$ when compared with its sibling, the LO PT term. The next goal is scanning the Borel parameter space in order to find a good Borel window, i.e., a range for τ where the sum-rule is reliable and gives the key settings to study its phenomenological side. Therefore,

the enhancement of the dispersion relations by selecting the proper range of τ is done by adjusting the total contribution of the gluon condensate to the sum-rule, also referred as the condition for the OPE convergence. In parallel with this process, the search for an optimal sum-rule parameter s_0 must be carried out by examining the energy spectrum and fixing the best value that minimizes the effects of excited states and the continuum, hence finding the best fit of the model.

To accomplish this objective, different criteria can be implemented in the QCDSR analysis, and this section will show the main results from some of these categories. The requirements chosen to constrain the Borel window are based in the search for an upper and lower bound, whereas other criteria are selected to find the optimal value of s_0. And finally, some tests are implemented to study the sensitivity of the results to small variations of these parameters. All of this will conclude with the σ mass prediction from two perspectives.

3.2.1 Sum-rule renormalization group equation

The sum-rules were tested by brute force (a primitive test by hand) under renormalization group equations (RGE) in order to check if the relation between $\mu^2_{\overline{MS}}$ is effectively held as $1/\tau$ as it was proposed in Ref. [101]. The solution of the RGE for Laplace sum-rule of light systems assuming that there is no anomalous dimension was applied, and it is the following expression (for simplicity in this section, $\mu^2_{\overline{MS}}$ is written simply as μ^2),

$$\mu^2 \frac{d}{d\mu^2}\left[\mathcal{R}_k(\tau, s_0, \mu^2)\right] = 0. \tag{3.13}$$

There must be a term $\mu^2\tau = \zeta > 0$, such that this relation above is satisfied. It is possible then to split the spectral function into the LO contributions and the NLO corrections. This is done because the only piece depending on the renormalization scale here are the NLO corrections, thus Eq. (3.13) was computed analytically in the following way:

$$\mathcal{R}_k(\tau, s_0, \mu^2) = \frac{1}{\pi}\int_{t_0}^{s_0} ds\, s^k\, e^{-s\tau}\, (\rho^{\mathrm{LO}}(s) + \rho^{\mathrm{NLO\ PT}}(s)), \tag{3.14}$$

then

$$\mu^2 \frac{d\,\mathcal{R}_k(\tau, s_0, \mu^2)}{d\,\mu^2} = \frac{1}{\pi}\mu^2 \frac{d}{d\,\mu^2}\left[\int_{t_0}^{s_0} ds\, s^k\, e^{-s\tau}\, \rho^{\text{NLO PT}}(s)\right]. \tag{3.15}$$

Here, the NLO part of the spectral function has the form:

$$\rho^{\text{NLO PT}}(s) = C_0 s^4 + A s^4 \alpha_s(\mu^2) + B s^4 \alpha_s(\mu^2) \log\Big(\frac{\mu^2}{s}\Big), \tag{3.16}$$

where the only terms depending on the renormalization scale parameter are the ones with the coefficients A and B.

$$A = \frac{409 - 192\sqrt{2}}{40\pi}, \qquad B = \frac{7 - 6\sqrt{2}}{4\pi}.$$

Hence, the derivative will go as

$$\mu^2 \frac{d\,\rho(s)}{d\,\mu^2} = \mu^2 \left[\frac{\partial \rho}{\partial \mu^2} + \frac{\partial \rho}{\partial \alpha_s}\frac{\partial \alpha_s}{\partial \mu^2}\right]. \tag{3.17}$$

On the one side, the first derivative term of Eq. (3.17) is

$$\frac{\partial \rho}{\partial \mu^2} = \frac{\partial}{\partial \mu^2}\Big(A s^4 \alpha_s\Big) + \frac{\partial}{\partial \mu^2}\left[B s^4 \alpha_s \log\left(\frac{\mu^2}{s}\right)\right] = \frac{B s^4 \alpha_s}{\mu^2}, \tag{3.18}$$

and on the other side, the second term is

$$\frac{\partial \rho}{\partial \alpha_s}\frac{\partial \alpha_s}{\partial \mu^2} = A s^4 \frac{\partial \alpha_s}{\partial \mu^2} + B s^4 \log\left(\frac{\mu^2}{s}\right)\frac{\partial \alpha_s}{\partial \mu^2}. \tag{3.19}$$

Hence, the total derivative is

$$\mu^2 \frac{d\,\rho(s)}{d\,\mu^2} = \mu^2 \left[\frac{B s^4 \alpha_s}{\mu^2} + A s^4 \frac{\partial \alpha_s}{\partial \mu^2} + B s^4 \log\left(\frac{\mu^2}{s}\right)\frac{\partial \alpha_s}{\partial \mu^2}\right], \tag{3.20}$$

where the derivative of the strong coupling was made using the definition in Eq. (3.11),

$$\frac{\partial \alpha_s(\mu^2)}{\partial \mu^2} = -\frac{25}{12\pi}\frac{1}{\mu^2}\alpha_s^2(\mu^2). \tag{3.21}$$

Replacing this into the RGE (Eq. (3.13)):

$$\mu^2 \frac{d\,\mathcal{R}_k}{d\,\mu^2} = \int_{t_0=0}^{s_0} ds\, s^k\, e^{-s\tau}\left[-\frac{25}{12\pi}A\alpha_s^2 s^4 - \frac{25}{12\pi}B\alpha_s^2 s^4 \log\Big(\frac{\mu^2}{s}\Big) + Bs^4\alpha_s\right] = 0. \tag{3.22}$$

Two types of integrals must be computed:

$$I_1 = \int_0^{s_0} ds\, s^{4+k}\, e^{-s\tau}, \tag{3.23}$$

$$I_2 = \int_0^{s_0} ds\, s^{4+k}\, e^{-s\tau}\, \log\Big(\frac{\mu^2}{s}\Big). \tag{3.24}$$

When taking the limit $s_0 \to \infty$, and $k = 0$:

$$I_1 = \int_0^{\infty} ds\, s^4\, e^{-s\tau} = \frac{4!}{\tau^{4+1}} = \frac{24}{\tau^5},$$
$$I_2 = -\int_0^{\infty} ds\, s^4\, e^{-s\tau}\, \log\Big(\frac{s}{\mu^2}\Big) = -\frac{50}{\tau^5} + \frac{24\gamma_E}{\tau^5} + \frac{24}{\tau^5}\,\log\big(\mu^2\tau\big),$$

where $\gamma_E \approx 0.577$ is the Euler-Mascheroni constant, and $\mu^2\tau = \zeta$.

Now, these integrals can be replaced into the definition of the RGE and this must be equal to zero, then

$$\mu^2 \frac{d\,\mathcal{R}_k}{d\,\mu^2} = \left[-\frac{25}{12\pi}A\alpha_s^2 + B\alpha_s\right]\frac{24}{\tau^5} + \frac{24}{12\pi}B\alpha_s^2\left[\frac{50}{\tau^5} - \frac{24\gamma_E}{\tau^5} - \frac{24}{\tau^5}\log(\zeta)\right] = 0. \tag{3.25}$$

The aim is to find a solution for $\mu^2\tau = \zeta$,

$$\frac{\alpha_s}{\pi}\left(25A - \frac{25^2 B}{12} + 25\gamma_E B + 25B\log(\zeta)\right) - 12B = 0. \tag{3.26}$$

It was found that this relation is not satisfied for any value of $\mu^2\tau = \zeta$, indicating that this result must be dependent on the anomalous dimension term from the RGE definition.

Strictly speaking, the total derivative in Eq. (3.13) is expanded as:

$$\left[\mu^2\frac{\partial}{\partial\mu^2}+\beta(\alpha_s)\,\frac{\partial}{\partial\alpha_s}+\gamma_m(\alpha_s)\frac{\partial}{\partial m_q}+\gamma_Z(\alpha_s)\right]\mathcal{R}_k(\tau,s_0)=0, \tag{3.27}$$

where $\beta(\alpha_s)$ and $\gamma_{m,Z}(\alpha_s)$ are universal functions related to the strong coupling constant in QCD [33, 36]. By definition $\beta(\alpha_s)$ is understood as the rate of change of the renormalized coupling at the μ^2 scale; $\gamma_m(\alpha_s)$ is related to the running quark masses, which are taken equal to zero for the analysis in the light sector; and $\gamma_Z(\alpha_s)$ is known as the anomalous dimension of the affected function, and its relation is directly connected to the renormalization constants.

In this scenario, where the anomalous dimension is included the sum-rules are re-written as:

$$\widetilde{\mathcal{R}}_k(\tau,s_0)=\left(\frac{\alpha_s}{\pi}\right)^{\nu}\mathcal{R}_k(\tau,s_0), \tag{3.28}$$

where ν stands for the sum-rule with the anomalous dimension included, and it is associated to the expansion in the strong coupling, whose origin comes from the loop diagrams and counterterms. It is evident here that the ratio of sum-rules stays protected independently of the value of the anomalous dimension.

$$\frac{\widetilde{\mathcal{R}}_{k+1}(\tau,s_0)}{\widetilde{\mathcal{R}}_k(\tau,s_0)}=\frac{\left(\frac{\alpha_s}{\pi}\right)^{\nu}\mathcal{R}_{k+1}(\tau,s_0)}{\left(\frac{\alpha_s}{\pi}\right)^{\nu}\mathcal{R}_k(\tau,s_0)}=\frac{\mathcal{R}_{k+1}(\tau,s_0)}{\mathcal{R}_k(\tau,s_0)},\qquad \text{for } k\geq 0. \tag{3.29}$$

In conclusion, the ratio of the sum-rules remains invariant even when considering the anomalous dimension as a part of the RGE requirements, from where it is relevant to stress that only ratios of the sum-rules are used in the phenomenological analysis of the single and double resonance models (see Eqs. (2.27) and (2.32)).

3.2.2 Gluon condensate

The Gluon condensate analysis is one of the chosen criteria to study QCDSR's, where the condition imposed lies in the desired proportion of the gluon condensate contribution with

respect to the PT terms within the sum-rule, in which case the term $\langle \alpha_s GG \rangle$ is expected to not exceed 1/3 of the total contribution from the PT terms [67, 92].

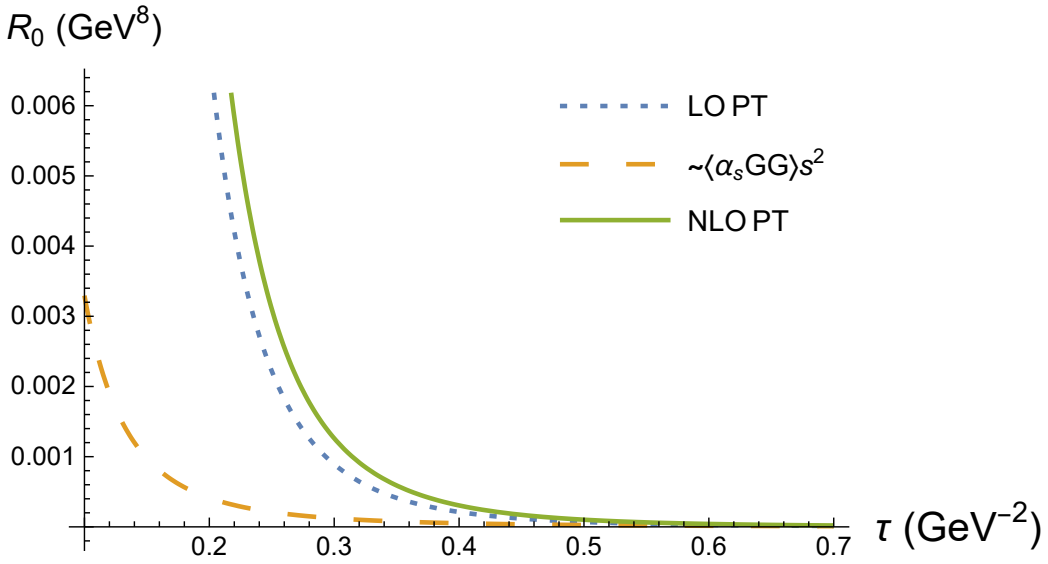

Figure 3.3: Individual contributions to the sum-rule $R_0(\tau, \infty)$ versus τ, for $\tau < 1$ GeV^{-2}.

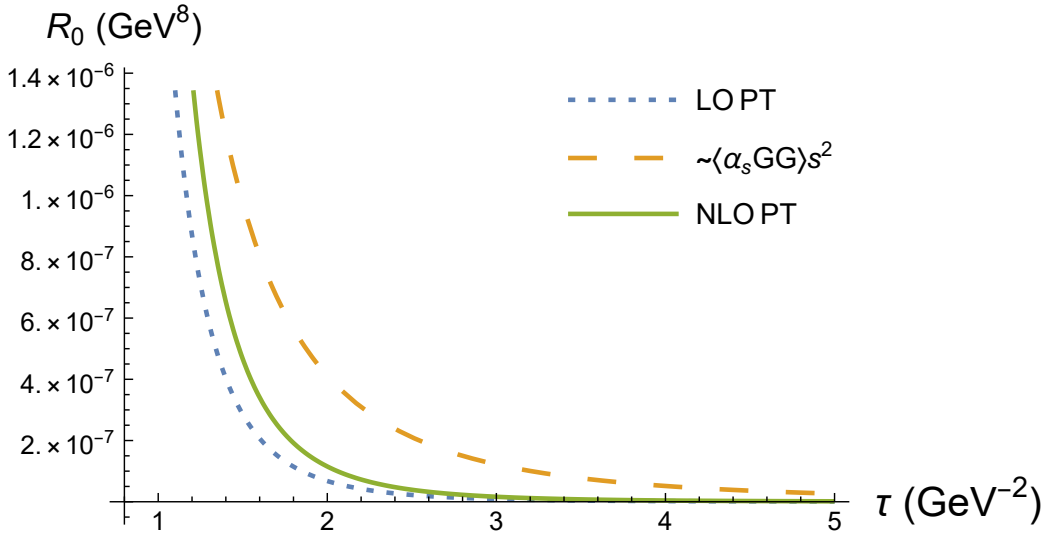

Figure 3.4: Individual contributions to the sum-rule $R_0(\tau, \infty)$ versus τ, for $\tau > 1$ GeV^{-2}.

Firstly, in order to discriminate certain regions in the τ-parameter space, the Laplace sum-rules were examined for a broad energy range using Eq. (2.26) and fixing $t_0 = 0$, because the physical threshold is linked to the quark content masses, in this case just restricted by light

quarks. The computation of $\mathcal{R}_0(\tau, s_0)$ and $\mathcal{R}_1(\tau, s_0)$ for a wide range of values of τ within the whole energy range ($s_0 \to \infty$) are shown in Figs. 3.3 to 3.6. Each separate curve represents each of the three main contributions from the spectral function $\rho(s)$. In these figures LO represents just the leading-order perturbative term and NLO represents up to next-to-leading order perturbative contributions.

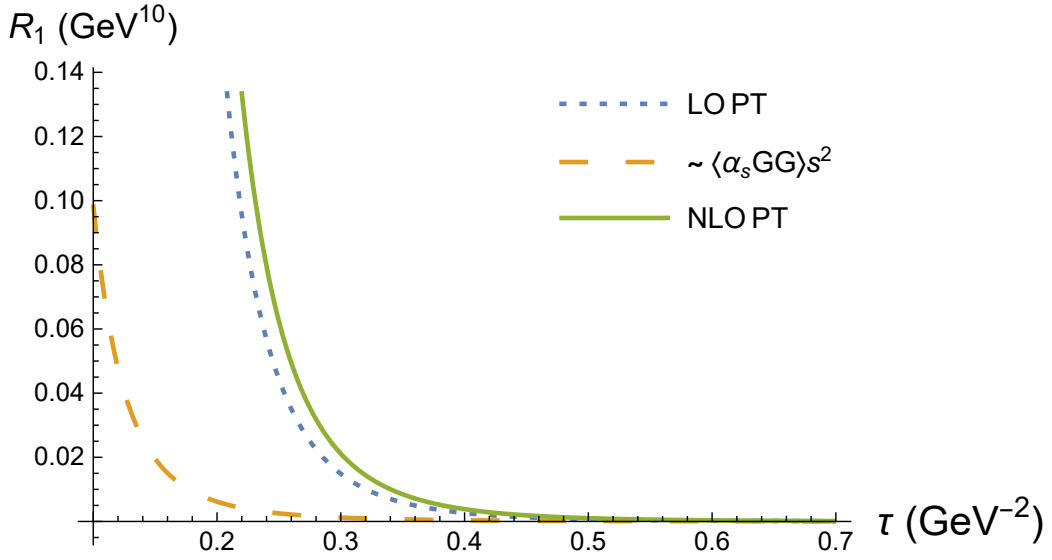

Figure 3.5: Individual contributions to the sum-rule $R_1(\tau, \infty)$ versus τ, for $\tau < 1$ GeV^{-2}.

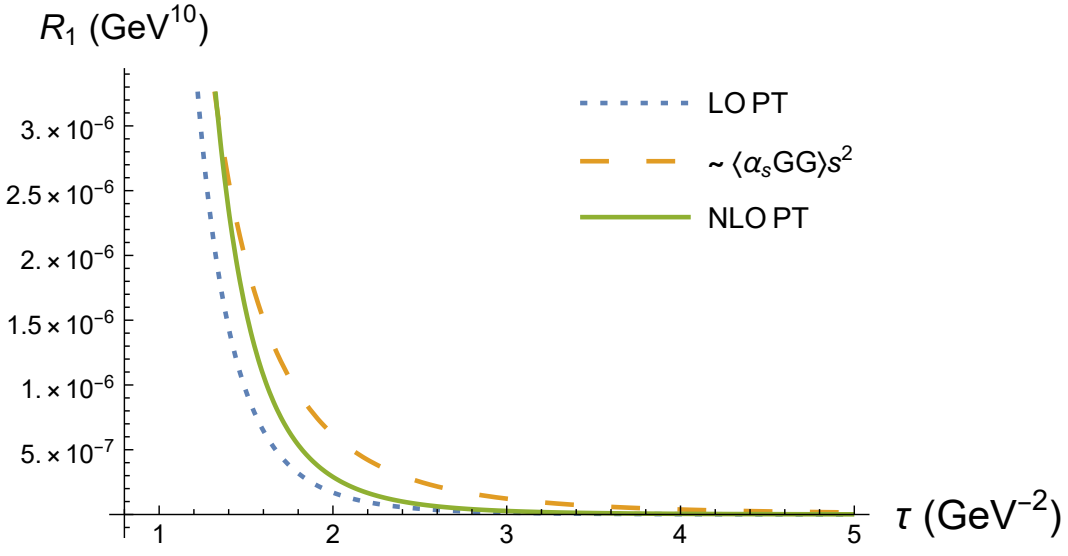

Figure 3.6: Individual contributions to the sum-rule $R_1(\tau, \infty)$ versus τ, for $\tau > 1$ GeV^{-2}.

There is a clear evidence that at small values of the Borel parameter ($\tau < 1$ GeV^{-2}) in Figs. 3.3 and 3.5, the contribution from $\langle\alpha_s GG\rangle$ (dashed orange line in plots) is smaller with respect to LO and NLO PT terms, thus constraining the Borel parameter to this range, and satisfying the requirement that PT terms must be dominant.

It is of great importance to mention that the results in Figs. 3.4 and 3.6 were chosen in order to show the contributions from the gluon condensate in terms of all the possible values that τ can take in this scene without ruling out any region yet. Some studies [11, 19, 74] suggest the Borel parameter to be within this range ($1\,\text{GeV}^{-2} < \tau < 5\,\text{GeV}^{-2}$), but the QCD physics starts being problematic in this region. The Borel parameter τ is related to the renormalization scale parameter through $\mu^2_{\overline{MS}} = 1/\tau$ [101], then recalling the definition of α_s in Eq. (3.11), it is evident that the choice of the renormalization scale has direct effect on the strong coupling and so does the choice of the Borel window. Hence, τ must match the region where the strong coupling is well-behaved and under control, i.e., $\mu^2_{\overline{MS}}$ cannot be too small such that PT can be applied, and this scale cannot be too large so the excited states and the continuum does not overwhelm the calculations.

Furthermore, given the definition of the hadronic mass, the physical mass prediction must be independent of this $\mu^2_{\overline{MS}}$ parameter, so independent of τ, whose role is defined as an auxiliary variable that should not impact the final results.

After shrinking the window of τ to values below 1 GeV^{-2}, the following conditions were imposed to constrain the Borel parameter by setting the upper bound:

$$B_k^{\langle\alpha_s GG\rangle/LO} = \left| \frac{\mathcal{R}_k^{\langle\alpha_s GG\rangle}(\tau,\infty)}{\mathcal{R}_k^{\text{LO PT}}(\tau,\infty)} \right| \leq \frac{1}{3}, \qquad \text{for } k \geq 0, \tag{3.30}$$

and

$$B_k^{\langle\alpha_s GG\rangle/NLO} = \left| \frac{\mathcal{R}_k^{\langle\alpha_s GG\rangle}(\tau,\infty)}{\mathcal{R}_k^{\text{LO+NLO PT}}(\tau,\infty)} \right| \leq \frac{1}{3}, \qquad \text{for } k \geq 0, \tag{3.31}$$

where $\mathcal{R}_k^{\langle\alpha_s GG\rangle}$ corresponds to the sum-rule piece made up of the gluon condensate term only, and $\mathcal{R}_k^{\text{LO PT}}$ and $\mathcal{R}_k^{\text{LO+NLO PT}}$ are referred to the PT terms of the total sum-rule. Equations (3.30) and (3.31) are expressed as ratios of sum-rules, which keeps the calculations safe

and consistent with the previous discussion. They were calculated for $k = 0, 1$, and their results are shown in Table 3.2.

k	$B_k^{\langle\alpha GG\rangle/LO}$	$B_k^{\langle\alpha GG\rangle/NLO}$
0	$\tau \leq 0.47$ GeV^{-2}	$\tau \leq 0.57$ GeV^{-2}
1	$\tau \leq 0.61$ GeV^{-2}	$\tau \leq 0.75$ GeV^{-2}

Table 3.2: Results of Eqs. (3.30) and (3.31) for $k = 0, 1$. These results show the shift on the upper bound for the Borel window when adding the NLO PT correction to the spectral function.

The advantage of the NLO PT term in this context is the resulting widened Borel window as shown in Table 3.2, where τ is shifted to a higher bound with the consequence of an improvement in the convergence of the OPE. The purpose of computing both Eqs. (3.30) and (3.31) was comparing the effective impact of the NLO PT terms in the QCDSR analysis and their corresponding parameters.

As a brief summary of the results of this section, a reasonable upper bound for the Borel window was found and it is restricted within a range of values below 1 GeV^{-2}, whose characteristics match the physical scenario and they satisfy the known constraints from theory. The NLO upper bound on $\tau \leq 0.57$ GeV^{-2} seems to be reliable in terms of the QCDSR approach.

3.2.3 Ratio of ratios

To continue with the analysis, the ratio of ratio of sum-rules was considered and implemented during the study of the QCDSR's and the search for a good Borel window. This approach was taken as a tool to have an unrefined picture of the effects of the NLO PT terms on the Laplace sum-rule using the results obtained in the previous section. Firstly, having established the upper bound on the Borel parameter and comparing the QCD Laplace sum-rules for LO and NLO spectral functions, the corresponding percentage of the NLO PT sum-rule with respect to the LO PT results are shown in Fig. 3.7.

Evidently the proportion of the NLO PT terms with respect to the LO PT terms in the sum-rule scheme supports the notion of these large contributions from the radiative corrections to the results, and independently of the value of τ within the Borel window the

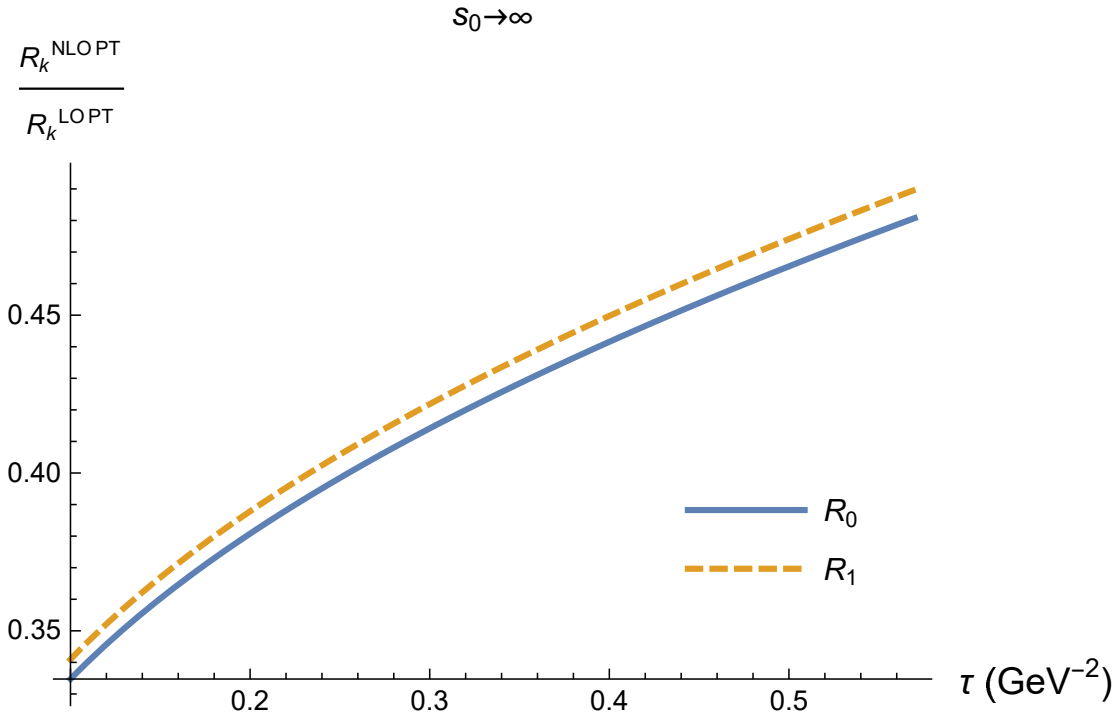

Figure 3.7: Percentage of the NLO PT terms with respect to LO PT terms within the sum-rule formulation at $s_0 \to \infty$ and considering the upper bound on $\tau \leq 0.57$ GeV^{-2}.

contribution remains more or less constant, between 40% to 50%.

Another strategy is presented in order to have an overview from another perspective on these contributions. Hence, the ratio of ratios is formulated as

$$\sqrt{\frac{\mathcal{R}_1^{LO}(\tau, s_0)}{\mathcal{R}_0^{LO}(\tau, s_0)}} \Bigg/ \sqrt{\frac{\mathcal{R}_1^{NLO}(\tau, s_0)}{\mathcal{R}_0^{NLO}(\tau, s_0)}}. \tag{3.32}$$

The ratio of ratios preserves the reliability of the calculations, since it keeps the results independent of possible anomalous dimension effects found in the previous sections.

It is crucial to remark that relation Eq. (3.32) can be interpreted from two different frameworks. First, from the single narrow resonance model (Eq. (2.27)), in which case this ratio will be equivalent to:

$$\frac{\mathcal{R}_1^{LO}(\tau, s_0)}{\mathcal{R}_0^{LO}(\tau, s_0)} \cdot \frac{\mathcal{R}_0^{NLO}(\tau, s_0)}{\mathcal{R}_1^{NLO}(\tau, s_0)} = \frac{(m_\sigma^2)^{LO}}{(m_\sigma^2)^{NLO}}, \tag{3.33}$$

and it is only valid if the sum-rules are including exclusively the single lightest resonance σ.

Second, this ratio of ratios can be generalized with the multiple narrow resonance model, highlighting that this proportion $\mathcal{R}_1(\tau, s_0)/\mathcal{R}_0(\tau, s_0)$ will not represent the hadronic mass itself, but somewhat of a sum of possible outcomes (Eq. (2.32)), where more than one state could be coupled to the same current.

The relevance of this comparison is tightly related to study the sensitivity of the ratio of the sum-rules with respect to the NLO PT terms, and their results are shown in Fig. 3.8.

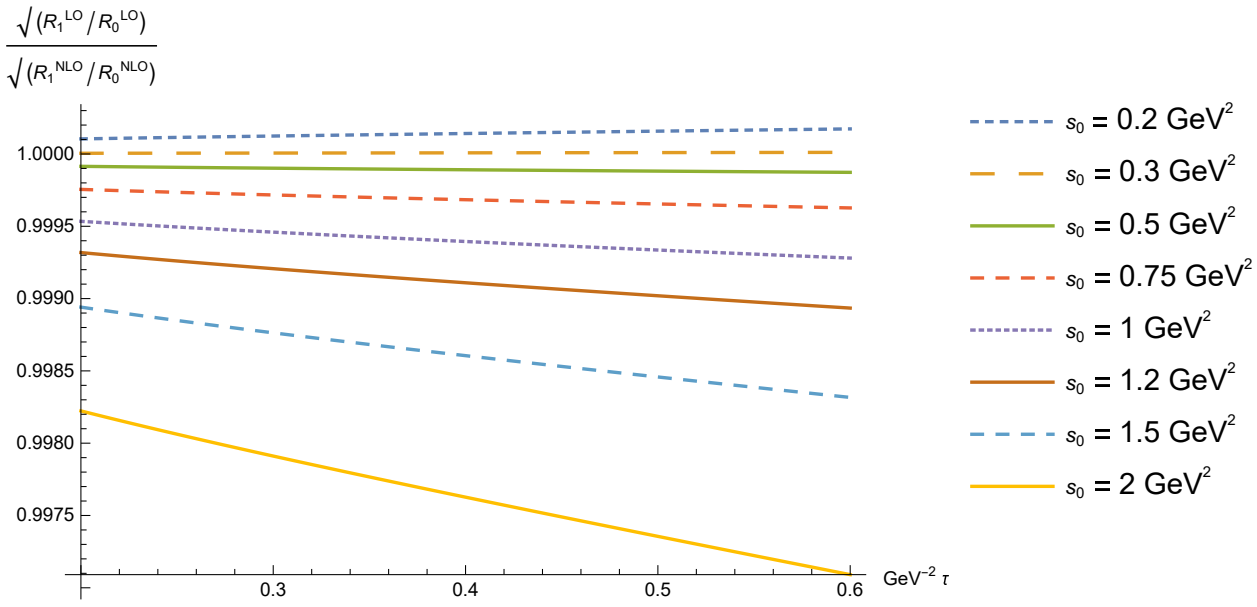

Figure 3.8: Ratio of the QCD Laplace sum-rule ratio of LO and NLO versus the Borel parameter $\tau < 1$ GeV^{-2} for different values of the continuum threshold s_0.

There is a distinct pattern in all these curves indicating that independently of the parameter space taken, the ratio in Eq. (3.32) remains approximately constant and very close to 1. Despite the important contributions of the NLO radiative corrections to the spectral function, these contributions seem to be compensated in the sum-rule ratio results by not increasing substantially the effects on the mass prediction calculations, but rather improving the sum-rule analysis by providing a more reliable Borel window to study.

In this matter, let us point out that the results from the ratio of the ratios of the sum-rules show strong insensitivity to the NLO PT terms within the constrained $\tau \leq 0.57$ GeV^{-2}, hence the QCDSR analysis relies upon a safe starting point for the Borel window, and this safety is reassured and preserved when working specifically with the ratios.

3.2.4 Hölder Inequalities

Hölder Inequalities are a methodology that helped finding a lower bound for the Borel parameter, as well as giving the basics to optimize the continuum threshold s_0 through the use of adequate χ^2 functions, where the optimal value for s_0 was fixed with the use of the Borel window $\tau_{\min} \leq \tau \leq \tau_{\max}$.

To begin with, this approach establishes the following conditions for the QCD Laplace sum-rules [102] to find $\tau_{\min}$,

$$\frac{\mathcal{R}_k\big(\tau + [1-\omega]\,\delta\tau, s_0\big)}{\mathcal{R}_k^{\omega}\big(\tau, s_0\big)\mathcal{R}_k^{1-\omega}\big(\tau + \delta\tau, s_0\big)} \leq 1, \quad \text{for} \quad 0 \leq \omega \leq 1, \text{ and } \; k \geq 0, \tag{3.34}$$

evaluated for $k = 0, 1$ and $\delta\tau = 0.05$ GeV^{-2} [102]. The upper bound $\tau_{\max}$ was found with the gluon analysis criterion, where the NLO PT terms have an significant role shifting the upper bound to a higher value of the Borel parameter in comparison with the analysis made without this term. Secondly, in order to confirm the results concerning the lower bound, the following relation was applied [103]

$$\frac{\mathcal{R}_k(\tau, s_0)/\mathcal{R}_{k-1}(\tau, s_0)}{\mathcal{R}_{k-1}(\tau, s_0)/\mathcal{R}_{k-2}(\tau, s_0)} \geq 1, \quad \text{for} \quad k \geq 2, \tag{3.35}$$

which was tested for $k = 2$. Results obtained from Eqs. (3.34) and (3.35) are shown in Table 3.3, where the value of the minimum s_0 was set.

Threshold (GeV^2)	Estimated τ (GeV^{-2})
Results from Eq. (3.34)	
$s_0 = 2$	τ =0.2
$s_0 = 1$	τ =0.2
$s_0 = 0.5$	$\tau = 0.25$
$s_0 = 0.4$	$\tau = 0.3$
$s_0 = 0.3$	Not found
Results from Eq. (3.35)	
$s_0 = 0.33$	$\tau = 0.2$

Table 3.3: Results for a lower bound on τ using Eq. (3.34) and (3.35), and placing the minimum squared energy at $s_0^{\min} = 0.33\,\text{GeV}^2$. Below this $s_0^{\min}$ the Hölder Inequalities fail, but they are somewhat constant for higher values of s_0.

Then combining the results of Tables 3.2 and 3.3, a good Borel window was found in the range:

$$0.2\ \text{GeV}^{-2} \leq \tau \leq 0.57\ \text{GeV}^{-2}. \tag{3.36}$$

These results makes physical sense, since the Borel parameter must be sufficiently large such that the lowest states possible are included and the continuum is highly suppressed, but due to its relation with the strong coupling, the value of τ must be confined to certain neighbourhood where $\alpha_s(\mu^2_{\overline{MS}} = 1/\tau)$ is still under control, i.e., the process must occur at low energy, yet in a sector where the strong coupling can be treated with PT.

After this whole process of scanning values of τ to get a proper range for the Borel window, the implementation of another criterion to examine the optimal s_0 must be applied. This optimal value s_0 determines the energy scale where the σ state can be studied preventing contamination from excited states. Therefore, s_0^{opt} was obtained by performing a fit with the minimization of specific χ^2 functions outlined below, which was made from the perspectives of the single and double narrow resonance analysis.

3.2.5 Single Resonance analysis (SR)

This model parametrizes the spectral function by considering a separation of the narrow resonance and the continuum within different energy ranges. The aim was to find an optimal value of s_0 to estimate m_σ in Eq. (2.29) making use of the Borel window found in the previous sections. This is obtained with the following definitions:

$$\chi^2_{\text{SR}}(s_0) = \sum_j \left(m_\sigma^2 \frac{\mathcal{R}_0(\tau_j, s_0)}{\mathcal{R}_1(\tau_j, s_0)} - 1 \right)^2; \quad s_0 \geq s^{min}. \tag{3.37}$$

$$\frac{d\,\chi^2_{\text{SR}}}{d\,m^2_\sigma} = 0, \qquad \frac{d\,\chi^2_{\text{SR}}}{d\,s_0} = 0, \tag{3.38}$$

where the label SR in χ_{SR} denotes single resonance, and this is done in order to seek the optimal s_0 so χ^2_{SR} is minimized.

The combination of these equations were used to perform the optimization, whose results

for the continuum threshold and mass estimates are shown in Figs. 3.9 and 3.10. These plots were computed using the inputs in Table 3.4.

Variable	Range
τ	$0.2 - 0.57$ GeV^{-2}
s_0	$0.33 - 1.3$ GeV^2
$\delta\tau$	0.05 GeV^2

Table 3.4: Inputs for Eq. (3.37) in order to minimize the $\chi^2_{\rm SR}$ function. The quantity $\delta\tau$ is defined by $\delta\tau = \tau_{j+1} - \tau_j$.

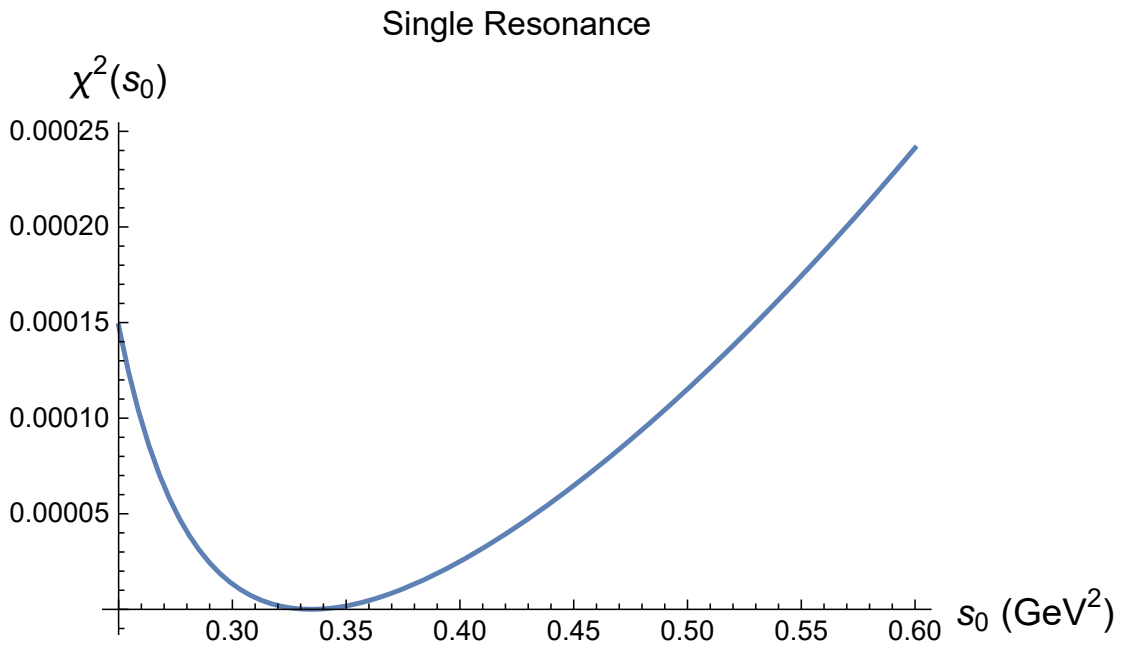

Figure 3.9: Plot of $\chi^2_{\rm SR}$ with respect to s_0 from the single narrow resonance model. The minimum found for the energy range below 1 GeV is critically near the Hölder Inequality threshold, at $s_0 = 0.335$ GeV^2.

The optimal s_0 found and the corresponding mass estimate are:

$$s_0 = 0.335 \text{ GeV}^2, \qquad m_\sigma = 0.52 \pm 0.01 \text{ GeV}. \tag{3.39}$$

The value of m_σ found is within the range given by Particle Data Group (PDG) [1] and is showing strong insensitivity to small variation of the Laplace sum-rule parameters s_0 and τ, the latter can be seen in Fig. 3.10, which were tested for changes up to 10%. The results seem to be correct in terms of the steps followed during the process and the extracted value of

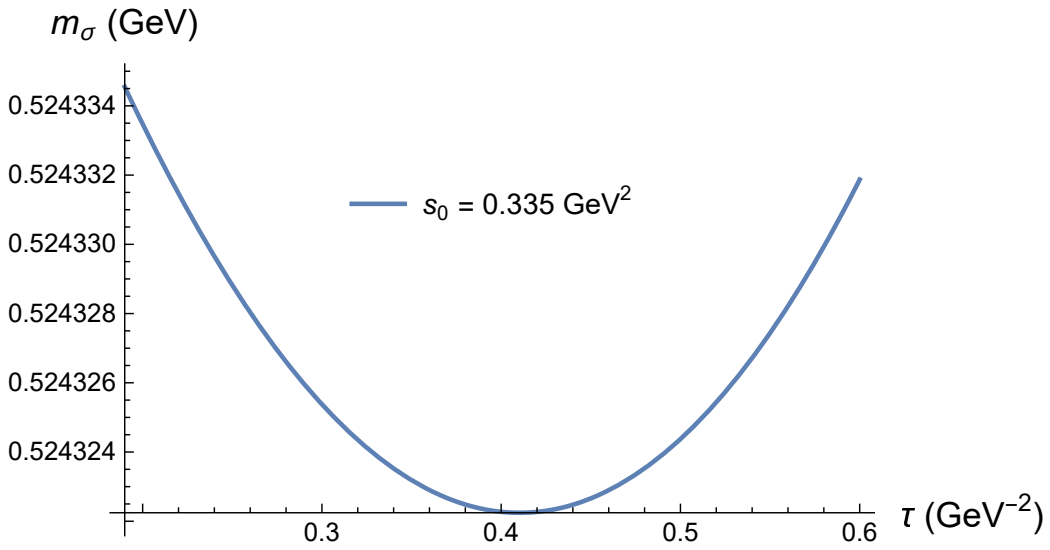

Figure 3.10: Mass prediction, m_σ from QCDSR analysis with a single resonance parametrized spectral function, positioning the pole at $m_\sigma = 0.52$ GeV.

the mass makes physical sense. However, the physical region that this continuum threshold was found is not quite convincing, since it is located near the lower limit on s_0 established in Table 3.3, this proximity of the continuum threshold to the Hölder inequality threshold motivates further investigation with a double resonance model.

The second resonance can in principle absorb some of the continuum, therefore possibly increasing the optimized s_0. The next section develops and details the double narrow resonance analysis.

3.2.6 Double Resonance analysis (DR)

This model contemplates an extra narrow resonance in the spectral function parametrization, where this new resonance is located near the lowest pole found, and it represents the next-heavier scalar ground state. This extension will transform the sum-rule as it was described in Eq. (2.32), where the lightest resonances studied are the σ and $f_0(980)$.

Thus, a χ^2 function was calculated with the following definition of the ratio of the sum-rules:

$$\frac{\mathcal{R}_1(\tau, s_0)}{\mathcal{R}_0(\tau, s_0)} = \frac{m_\sigma^2 + r\, m_{f_0}^2\, e^{-\Delta m^2 \tau}}{1 + r\, e^{-\Delta m^2 \tau}}, \tag{3.40}$$

and the expressions below were replaced in Eq. (2.32):

$$r = \frac{A_{f_0}}{A_\sigma}, \qquad \Delta m^2 = m_{f_0}^2 - m_\sigma^2,$$

r is the ratio of the resonance strengths, Δm^2 is the difference of the squared masses of the states of interest, and $m_{f_0} = 0.98$ GeV is the mass of $f_0(980)$, considered as a fixed value, since it has been well-studied and the uncertainties on its mass prediction are small [1]. Hence, the optimization will be over

$$\chi^2_{\rm DR}(s_0) = \sum_j \left(m_\sigma^2 \frac{\mathcal{R}_0(\tau_j, s_0)}{\mathcal{R}_1(\tau_j, s_0)} - 1 + r\, m_{f_0}^2\, e^{-\Delta m^2 \tau_j} \frac{\mathcal{R}_0(\tau_j, s_0)}{\mathcal{R}_1(\tau_j, s_0)} - r\, e^{-\Delta m^2 \tau_j} \right)^2; \quad s_0 \geq s^{min}, \tag{3.41}$$

where the label DR denotes double resonance.

Notice that in the case that $A_{f_0} = 0$ then $r = 0$, i.e., the second resonance does not couple to the current, and the expression for the single narrow resonance Eq. (3.37) is recovered. Hence Eq. (3.41) is a natural extension of Eq. (3.37).

Equation (3.41) was minimized with respect to m_σ^2 and r to get the optimal s_0:

$$\frac{\partial \chi^2_{\rm DR}}{\partial m_\sigma^2} = 0, \qquad \frac{\partial \chi^2_{\rm DR}}{\partial r} = 0, \qquad \frac{\partial \chi^2_{\rm DR}}{\partial s_0} = 0. \tag{3.42}$$

From these equations, expressions for the $\chi^2_{\rm DR}(s_0)$ function and the ratio $r(s_0)$ were obtained and plotted against the energy range s_0.

The optimization was made using the inputs shown in Table 3.5, where the results are selected according to the minimum value of the $\chi^2_{\rm DR}$ function when changing the ranges of m_σ and s_0 shown below.

The plot in Fig. 3.11 displays two minimum, the first minimum is local and around $0.6 - 0.8$ GeV^2, whereas the global deeper minimum is placed at $1 - 1.2$ GeV^2.

Within these calculations, let us remark that the continuum threshold s_0 found shows a strong insensitivity to the changes of Borel window and to the changes of $\delta\tau$ of up to 10%, hence, satisfying one of the main requirements of the QCDSR approach, the stability of the results around the fixed s_0.

The value of the continuum threshold found was consistent with $f_0(980)$, above 0.98 GeV.

Variable	Range
s_0	$0.33 - 1.3\ \mathrm{GeV}^2$
τ	$0.2 - 0.57\ \mathrm{GeV}^{-2}$
m_σ	$0.45 - 0.8\ \mathrm{GeV}$
$\delta\tau$	$0.05\ \mathrm{GeV}^{-2}$

Table 3.5: Inputs given to $\chi^2_{\mathrm{DR}}(s_0)$. The starting point of the range of s_0 was chosen in a low energy sector in order to compare with the single narrow resonance minimum obtained previously. However, given the physical conditions, and the $f_0(980)$ included as the second resonance, the results must be studied from $s_0 = 1\,\mathrm{GeV}^2$.

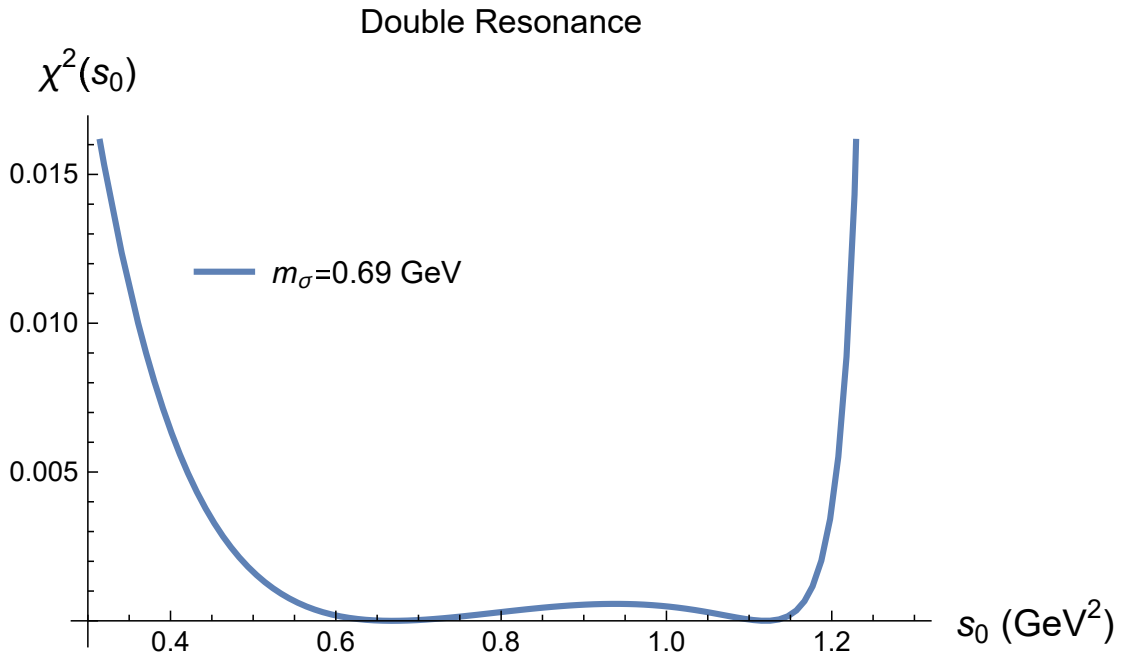

Figure 3.11: χ^2_{DR} optimization of continuum threshold from a double narrow resonance analysis, whose global minimum is located at $s_0 = 1.12\,\mathrm{GeV}^2$.

The optimal s_0 and m_σ are:

$$s_0 = 1.12\,\mathrm{GeV}^2, \qquad m_\sigma = 0.69 \pm 0.03\,\mathrm{GeV}. \tag{3.43}$$

Additionally, the other important variable calculated is the ratio $r(s_0)$ with the continuum threshold and m_σ defined:

$$r(s_0) = \frac{A_{f_0}}{A_\sigma} = 3.38. \tag{3.44}$$

The variation of this ratio versus the energy is shown in Fig. 3.13.

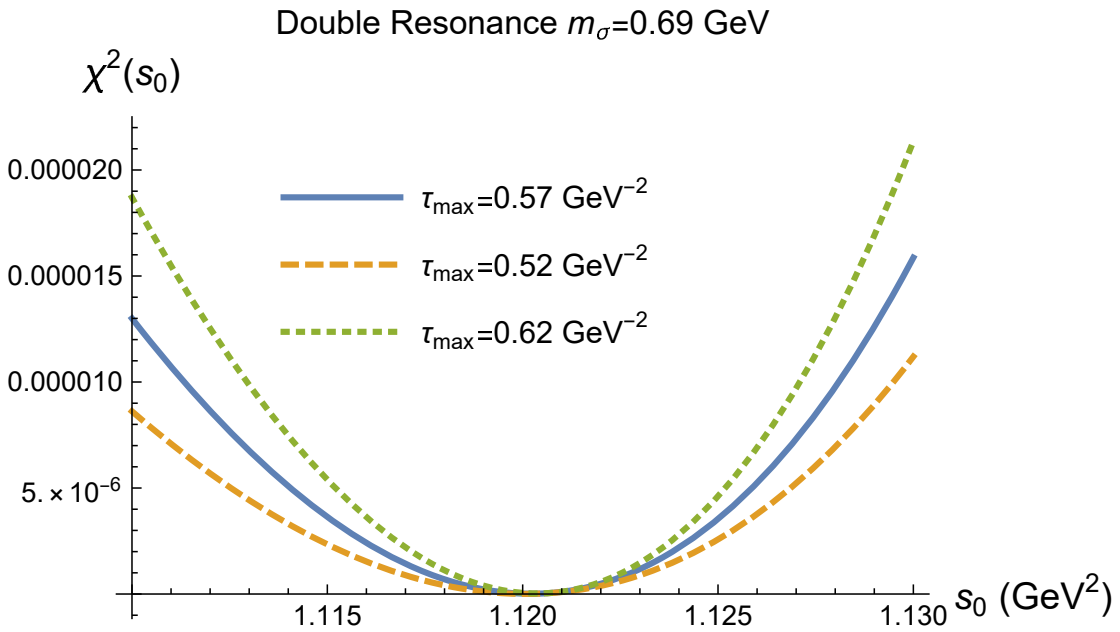

Figure 3.12: s_0 stability in the minimization of $\chi^2_{\rm DR}$ under small variations on the upper bound of the Borel window τ.

This result for r is related to the resonance strengths with which both states couple to the current studied, and it means that the heavier $f_0(980)$ state couples more strongly in comparison with the σ, hence the sum-rule is sensitive to the presence of $f_0(980)$, but in which case these results are in great agreement with the mixing of these two states found from the studies using chiral lagrangians, which suggest the mixing angle enhances the coupling of the scalar $f_0(980)$ [78, 79].

3.3 Discussion

This thesis studied the contribution from NLO diagrams to the spectral functions of the lowest-lying state belonging to the lightest scalar nonet (σ), which is expected to have a strong tetraquark component according to some studies [77–79]. The results showed an important contribution from these NLO radiative corrections to the spectral function, up to 74% at low-energy and up to 40% at the energy limit where the light scalars are studied ($s = 2$ GeV^2). This significant contribution seems to be somehow overshadowed by the gluon condensate at low-energy regime as predicted by [11, 74], whose results of the hadronic masses of the lightest states in the chiral limit are dictated by the contribution of the gluon condensate

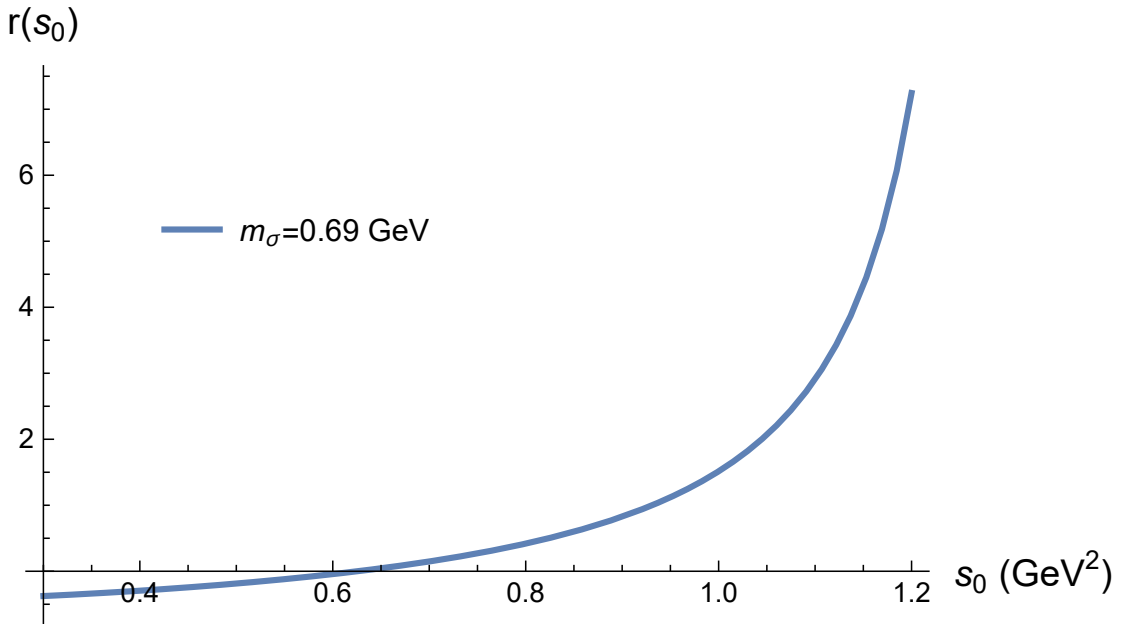

Figure 3.13: Ratio $r(s_0) = \frac{A_{f_0}}{A_\sigma}$ of the resonance strengths to the tetraquark current.

within the tetraquark scheme, but which weight becomes less important at higher-energy, and ultimately allows the observation of the enhancement from the NLO corrections.

The Laplace sum-rules obtained were consistent with the results from the spectral function, meaning, they were significantly affected by these contributions, where the sum-rule containing exclusively the NLO PT terms turns out to be up to 48% of the sum-rule containing the LO PT (see Fig. 3.7).

In addition, given the findings with the RGE testing in section 3.2.1, the sum-rules formulation must be treated using ratios of $\mathcal{R}_k(\tau, s_0)$, due to their possible dependence on the anomalous dimension, whose dependence vanishes when working with the ratios and so keeping the calculations in a reliable setting. Furthermore, the ratios of the total sum-rules, i.e., the ratio of the expressions containing all the contributions from perturbation theory plus the condensates (non-perturbative) appear to be insensitive to the NLO corrections, this behaviour is explained because the numerator and denominator contain these large corrections, hence this ends up having a compensation on both sides leaving the sum-rule ratio constant as shown in Fig. 3.8.

After performing these previous tests on the sum-rule ratios, a suitable Borel window was found by imposing the gluon condensate condition (OPE convergence requirement) and

Hölder Inequalities criteria. Here, it is vital to remark that even though the ratio of the sum-rules seems to be insensitive to the NLO corrections, the search for a good Borel window relies substantially on these NLO corrections, because of their effects on the upper limit of the Borel parameter τ, which is shifted to a higher bound thanks to this term and benefits the analysis by improving the convergence of the OPE and the implementation of the method giving a wider region to study these light states. From the gluon condensate constraint, the upper bound on τ was set at $\tau \leq 0.57$ GeV^{-2}, which is congruent with the physical region where these states are located. Furthermore, the lower bound on the Borel parameter was set using the Hölder Inequalities, which placed this value at $\tau \geq 0.2$ GeV^{-2}.

From the Hölder Inequalities perspective, the lower bound for τ was found using two constraints, which agreed on locating the minimum continuum threshold where the method is valid at $s_0 = 0.33\,\text{GeV}^2$. It is important to note that the minimum value of s_0 through the use of Eqs. (3.34) and (3.35) is very sensitive to small changes, and the results begin to deviate at order $(\delta\tau)^2$, hence reasonable numerical precision is needed for the choice of $\delta\tau$. Later by making use of the χ^2 optimization functions (Eqs. (3.37) and (3.41)), the continuum threshold was optimized within two scenarios, the resonance plus continuum models with single and double narrow resonances.

Concerning the mass predictions, the analysis gave results that are in agreement with the accepted values in PDG [1], however there are certain subtleties that can make changes in the predictions and must be considered. The approach to the physical situation from the single narrow resonance model can give a clue that the process and the Borel window were correctly chosen and the results were $m_\sigma = 0.52\,\text{GeV}$ and $s_0 = 0.335$ GeV^2, but one should not ignore the physical aspects of these results, namely, the continuum threshold found merits closer examination due to its proximity to the Hölder Inequality threshold ($s_0^{\text{min}} = 0.33$ GeV^2). Nevertheless, the method is highly efficient meeting the theoretical constraints such as the stability of the results around the vicinity of the continuum threshold and their insensitivity dealing with small variations of $\tau\,(\pm 0.05\,\text{GeV}^{-2})$.

Subsequently, a follow-up analysis was made within the double narrow resonance framework, in which case the heavier scalar resonance considered was $f_0(980)$. This analysis concluded that the results for the continuum threshold was $s_0 = 1.12$ GeV^2. After opti-

mizing the continuum threshold, the mass prediction was performed by minimizing the χ^2 optimization function, which led to a mass estimate of $m_\sigma = 0.69$ GeV, and being in agreement with Ref. [1] considering the Breit-Weigner resonance model. Additionally, the ratio r of the resonance strengths of both states was calculated with the use of the optimal value of s_0 and resulted in $r = 3.38$, indicating that the heavier state $f_0(980)$ couples more strongly to the current, which is expected from a chiral Lagrangian approach [78, 79].

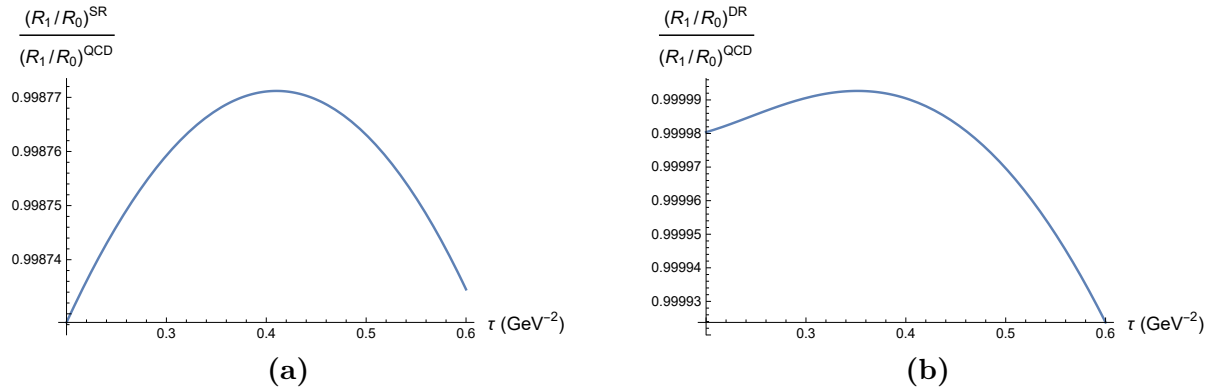

Figure 3.14: Ratio of the models versus the QCD predictions using the single narrow resonance (left) and the double narrow resonance (right), showing both estimations are good fits.

Fig. 3.14 shows the fit quality from the single narrow resonance (Fig. 3.14a) and double narrow resonance (Fig. 3.14b) models when compared to the QCD theoretical calculations. Both plots seem to model very well the situation, however the double resonance analysis shows a better fit and optimization across the values of the Borel window and manifests higher precision, while the single resonance model has its best behaviour in the central values of the Borel window, yet it still has a good accuracy considering the approximations made and the simplicity of the model.

This thesis found the σ mass prediction between $0.52\,\text{GeV} < m_\sigma < 0.69$ GeV, which could be interpreted as a variation of about $\sim 10 - 20\%$ around a central value. This is a robust estimation of the hadronic mass, it is reliable in every step and consistent with the physical constraints. Both models were taken as complementary methodologies to overcome certain weaknesses of each. The single narrow resonance results on the σ mass were reliable and it gave a good picture in terms of the chosen bounds for the Borel parameter τ, as well as the explicit insensitivity to its small variations, but its reliability was challenged with the

continuum threshold value. On the other hand, from the double narrow resonance model, the σ visibility is somewhat obscured by the presence of $f_0(980)$ in the picture, which seems to couple strongly to the chosen current. Moreover, the σ mass prediction and the use of the double resonance model and their adjustments manifested excellent agreement with the QCDSR predictions.

It it important to mention that Refs. [19, 74] predicted the σ mass using only the LO contributions to the spectral function, and because of a small $\langle\alpha_s GG\rangle$ value which has now been superseded their Borel window was chosen significantly larger than the one chosen in this thesis, yet both approaches agreed in the mass prediction range and they also match the prediction from models with chiral Lagrangians [78, 79].

Finally, as a summary for this section, the results obtained from both models are presented in Table 3.6.

Approach	range s_0 (GeV^2)	range τ (GeV^{-2})	m_σ (GeV)	s_0^{opt} (GeV^2)
SR	$0.33 - 1.3$	$0.2 - 0.57(\pm 0.05)$	0.52 ± 0.01	0.335
DR	$0.33 - 1.3$	$0.2 - 0.57(\pm 0.05)$	0.69 ± 0.03	1.12

Table 3.6: Summary of the results from QCDSR analysis with the results of the mass predictions from a single narrow resonance (SR) and double narrow resonance (DR) models.

In conclusion, the main goal of this thesis was achieved by demonstrating that the inclusion of the NLO diagrams have considerable effects on the spectral functions and the Laplace sum-rules, and subsequently in the choice of a proper Borel window, then affecting indirectly but fundamentally the mass prediction of the lightest scalar σ. Let us highlight that the main role of these radiative corrections showed their relevance by making possible the study of the scalar σ from the QCDSR approach within a reliable τ parameter space.

4 Conclusion

Tetraquark states had been of wide interest with the latest improvements and discoveries in collider physics and there has been a lot of controversy focused on the light scalar sector, which is the topic addressed in this thesis. The scalar σ has its complexity tightly linked to the low energy sector, due to its difficulty to distinguish it from the background. In this sense, it was found that the σ not only presents issues when trying to separate it form the background, but also when distinguishing from other scalar states due to the resonance strength coupling to the currents under investigation, which happens to be smaller than the next-heavier scalar $f_0(980)$ added to the analysis. Despite this, the mass prediction calculation found its light at the end of the tunnel, and showed key aspects to account for when computing it and the respective relevance of the NLO corrections in the QCDSR scheme.

As a summary, the analysis of the σ mass was tackled from the single narrow resonance and the double narrow resonance models, which provided important constraints for isolating the state from the background. The mass predictions from the point of view of both models showed indirect, but crucial dependence on the NLO corrections [11], which was manifested in the suitability to study the σ scalar from the QCDSR approach in the tetraquark picture.

The single narrow resonance was extended to the double narrow resonance analysis considering $f_0(980)$ as the next-heavier state, whose characteristics are well-known and so, their properties were used as inputs in the calculations. The double resonance analysis defined an extra parameter r, corresponding to the relative resonance strengths of the σ and $f_0(980)$ to the studied current. The predicted result in this thesis is $r = 3.38$, in good agreement with the evidence provided in Refs. [78, 79] from a chiral Lagrangian perspective whose results showed that r might be greater than 1.

The QCD Laplace sum-rules were tested under renormalization group equations, which exposed a possible dependence of the NLO PT corrections on the anomalous dimension.

However, these anomalous dimension effects were overcame by working with the ratio of the sum-rules, which kept the calculations reliable by cancelling this dependence. Although the NLO corrections did not show notable presence in the ratio of the sum-rules, their inclusion in the analysis gave a reliable Borel window for the QCDSR and improved the convergence of the OPE.

Additionally, this thesis presented the unique feature of working with the Hölder Inequalities method, which stands out for being a model-independent approach constraining the Borel window [102, 103]. This constraints were strict with the location of the lower bound of the Borel window and setting the minimal value of the continuum threshold.

The final results revealed high insensitivity to the variation of the QCDSR parameters, such as the continuum threshold s_0 and τ, and the mass estimation obtained $0.52\,\text{GeV} < m_\sigma < 0.69\,\text{GeV}$ was found within the range given by Ref. [1]. This result is surprisingly robust under superficially large NLO contributions, which added substantial weight to the spectral densities (up to 74%) and sum-rules (up to $40 - 50\%$), but whose weight was not directly seen as an explicit dominant term in the final mass prediction. However, due to these corrections the reliability of the study was present in the choice of a proper Borel window, $0.2\,\text{GeV}^{-2} \leq \tau \leq 0.57\,\text{GeV}^{-2}$, whose physical meaning is related to the renormalization scale parameter $\mu^2_{\overline{MS}}$, then making the study consistent in terms of the energy scale.

It is noteworthy to mention that even though certain approximations were made within this study, both models estimated the mass m_σ with remarkably good precision and made clear the importance of the NLO diagrams in the light scalar sector. The simplicity and accuracy of these models motivates the interest to extend the analysis by including an estimation of the effects of the σ width on the results. In addition to this extension, it would be interesting to use more complex models that include the single resonance and its relative weight in the sum-rule compared to the next-heavier scalar $f_0(980)$. Furthermore, the results of this research strongly encourages the use of this methodology with other channels, i.e., on other quantum numbers belonging to the light scalar nonet and study the prevalence of NLO effects in this sector.

Bibliography

[1] Particle Data Group, P. A. Zyla *et al.*, PTEP **2020**, 083C01 (2020).

[2] N. Brambilla, S. Eidelman, C. Hanhart, A. Nefediev, C.-P. Shen, C. E. Thomas, A. Vairo, and C.-Z. Yuan, Phys. Rept. **873**, 1 (2020).

[3] R. K. Ellis, W. J. Stirling, and B. R. Webber, *QCD and collider physics* (Cambridge university press, 2003).

[4] G. Cowan and T. Gershon, *Tetraquarks and pentaquarks* (IOP Publishing, 2018).

[5] Y.-R. Liu, H.-X. Chen, W. Chen, X. Liu, and S.-L. Zhu, Prog. Part. Nucl. Phys. **107**, 237 (2019).

[6] W. Lucha, D. Melikhov, and H. Sazdjian, PoS **EPS-HEP2019**, 536 (2020).

[7] C. Amsler and N. A. Törnqvist, Physics reports **389**, 61 (2004).

[8] E. Klempt and A. Zaitsev, Phys. Rept. **454**, 1 (2007).

[9] S. L. Olsen, Frontiers of Physics **10**, 121–154 (2015).

[10] G. Isidori *et al.*, Physics Letters B **662**, 424 (2008).

[11] S. Groote, J. Körner, and D. Niinepuu, Physical Review D **90** (2014).

[12] R. M. Albuquerque, S. Narison, A. Rabemananjara, D. Rabetiarivony, and G. Randriamanatrika, Phys. Rev. D **102**, 094001 (2020).

[13] J. Vijande, A. Valcarce, F. Fernandez, and B. Silvestre-Brac, Phys. Rev. D **72**, 034025 (2005).

[14] J. R. Peláez, Physics Reports **658**, 1–111 (2016).

[15] F. E. Close and N. A. Törnqvist, Journal of Physics G: Nuclear and Particle Physics **28**, R249–R267 (2002).

[16] Törnqvist, Nils A., Soryushiron Kenkyu **102**, 224 (2000).

[17] Törnqvist, Nils A., The Lightest scalar nonet, in *International Workshop on Chiral Fluctuations in Hadronic Matter*, 2002, hep-ph/0201171.

[18] J. Londergan, J. Nebreda, J. Pelaez, and A. Szczepaniak, Physics Letters B **729**, 9–14 (2014).

[19] H.-X. Chen, A. Hosaka, and S.-L. Zhu, Physical Review D **76** (2007).

[20] J. R. Peláez and G. Ríos, Physical Review Letters **97** (2006).

[21] I. Caprini, Physical Review D **77** (2008).

[22] R. Garcia-Martin, R. Kamiński, J. R. Peláez, and J. Ruiz de Elvira, Phys. Rev. Lett. **107**, 072001 (2011).

[23] D. V. Bugg, J. Phys. G **34**, 151 (2007).

[24] W. N. Cottingham and D. A. Greenwood, *An introduction to the standard model of particle physics* (Cambridge university press, 2007).

[25] L. H. Ryder, *Quantum field theory* (Cambridge university press, 1996).

[26] G. Ecker, *Particles, Fields, Quanta* (Springer, 2019).

[27] J. C. Romao and J. P. Silva, Int. J. Mod. Phys. A **27**, 1230025 (2012).

[28] ATLAS, G. Aad *et al.*, Phys. Lett. B **716**, 1 (2012).

[29] CMS, S. Chatrchyan *et al.*, Phys. Lett. B **716**, 30 (2012).

[30] J. F. Gunion, H. E. Haber, G. Kane, and D. Sally, *The Higgs hunter's guide* (CRC Press, 2018).

[31] P. W. Higgs, Phys. Lett. **12**, 132 (1964).

[32] CERN, The brout-englert-higgs mechanism, https://home.cern/science/physics/higgs-boson.

[33] M. Peskin and D. V. Schroeder, *An Introduction To Quantum Field Theory* (CRC Press, 2018).

[34] A. Ayala, Lecture notes in heavy-ion physics, https://indico.cern.ch/event/700261/, 2018.

[35] G. Zweig, *An SU(3) model for strong interaction symmetry and its breaking. Version 2* (CERN, 1964), pp. 22–101.

[36] Pascual, P. and Tarrach, R. *QCD: Renormalization for the practitioner* Vol. 194 (Springer, 1984).

[37] O. W. Greenberg, Physical Review Letters **13**, 598 (1964).

[38] O. W. Greenberg, Quarks and quantum statistics, 2010.

[39] Y. Ne'eman, Nucl. Phys. **26**, 222 (1961).

[40] J. Sakurai, Annals of Physics **11**, 1 (1960).

[41] S. Sakata, Progress of Theoretical Physics Supplement **19**, 3 (1961).

[42] M. Gell-Mann, Physics Letters **8**, 214 (1964).

[43] J.-M. Richard, An introduction to the quark model, in *Ferrara International School Niccolò Cabeo 2012: Hadronic spectroscopy*, 2012, arXiv:1205.4326.

[44] A. Chodos, R. Jaffe, K. Johnson, C. B. Thorn, and V. Weisskopf, Physical Review D **9**, 3471 (1974).

[45] S.-K. Choi *et al.*, Physical Review Letters **91** (2003).

[46] J. Z. Bai *et al.*, Physical Review Letters **91** (2003).

[47] M. Ablikim *et al.*, Physical Review Letters **95** (2005).

[48] M. Ablikim *et al.*, Physical Review Letters **106** (2011).

[49] K. Abe *et al.*, Physical Review Letters **98** (2007).

[50] R. Aaij *et al.*, Physical Review D **102**, 112003 (2020).

[51] R. Aaij *et al.*, Physical review letters **125**, 242001 (2020).

[52] LHCb, R. Aaij *et al.*, Sci. Bull. **65**, 1983 (2020).

[53] M. Ablikim *et al.*, Physical Review Letters **100** (2008).

[54] S.-K. Choi *et al.*, Physical Review Letters **94** (2005).

[55] Z. Q. Liu *et al.*, Physical Review Letters **110** (2013).

[56] X. Wang *et al.*, Physical Review D **91**, 112007 (2015).

[57] R. Aaij *et al.*, Physical Review Letters **112** (2014).

[58] R. M. Albuquerque, J. M. Dias, K. Khemchandani, A. Martínez Torres, F. S. Navarra, M. Nielsen, and C. M. Zanetti, J. Phys. G **46**, 093002 (2019).

[59] Belle, S. Uehara *et al.*, Phys. Rev. Lett. **96**, 082003 (2006).

[60] B. Aubert *et al.*, Physical Review Letters **90** (2003).

[61] M. Karliner, J. L. Rosner, and T. Skwarnicki, Ann. Rev. Nucl. Part. Sci. **68**, 17 (2018).

[62] S. L. Olsen, T. Skwarnicki, and D. Zieminska, Rev. Mod. Phys. **90**, 015003 (2018).

[63] T. Xiao, S. Dobbs, A. Tomaradze, and K. K. Seth, Phys. Lett. B **727**, 366 (2013).

[64] M. Ablikim *et al.*, Physical review letters **111**, 242001 (2013).

[65] LHCb, R. Aaij *et al.*, (2021), arXiv:2109.01056.

[66] LHCb, R. Aaij *et al.*, (2021), arXiv: 2109.01038.

[67] W. Chen, H.-X. Chen, X. Liu, T. Steele, and S.-L. Zhu, Phys. Rev. D **96**, 114017 (2017).

[68] W. Chen, H.-X. Chen, X. Liu, T. Steele, and S.-L. Zhu, Phys. Rev. D **95**, 114005 (2017).

[69] W. Chen, H.-X. Chen, X. Liu, T. Steele, and S.-L. Zhu, Physics Letters B **773**, 247–251 (2017).

[70] Z.-G. Wang, The European Physical Journal C **77**, 1 (2017).

[71] R. M. Albuquerque, S. Narison, D. Rabetiarivony, and G. Randriamanatrika, Doubly hidden 0^{++} molecules and tetraquarks states from QCD at NLO, 2021.

[72] R. Albuquerque, S. Narison, D. Rabetiarivony, and G. Randriamanatrika, Nuclear Physics A **1007**, 122113 (2021).

[73] D. Bugg, Physics Reports **397**, 257–358 (2004).

[74] H.-X. Chen, A. Hosaka, and S.-L. Zhu, Physics Letters B **650**, 369–372 (2007).

[75] R. L. Jaffe, Phys. Rev. D **15**, 267 (1977).

[76] G. Eichmann, C. S. Fischer, and W. Heupel, Phys. Lett. B **753**, 282 (2016).

[77] D. Black, A. H. Fariborz, F. Sannino, and J. Schechter, Physical Review D **59** (1999).

[78] A. H. Fariborz, International Journal of Modern Physics A **19**, 2095–2112 (2004).

[79] A. H. Fariborz, R. Jora, and J. Schechter, Physical Review D **79** (2009).

[80] F.-K. Guo, C. Hanhart, U.-G. Meißner, Q. Wang, Q. Zhao, and B.-S. Zou, Reviews of Modern Physics **90** (2018).

[81] W. H. Liang and E. Oset, Phys. Lett. B **737**, 70 (2014).

[82] D. Black, A. H. Fariborz, and J. Schechter, Soryushiron Kenkyu **102**, 115 (2000).

[83] M. A. Shifman, A. I. Vainshtein, and V. I. Zakharov, Nuclear Physics B **147**, 385 (1979).

[84] M. A. Shifman, A. Vainshtein, and V. I. Zakharov, Nuclear Physics B **147**, 448 (1979).

[85] C. A. Dominguez, *Quantum Chromodynamics Sum Rules* (Springer, 2018).

[86] J. Ellis, Comput. Phys. Commun. **210**, 103 (2017).

[87] M. Shifman, Czechoslovak Journal of Physics **52**, B102 (2002).

[88] J. Sakurai, Physics Letters B **46**, 207 (1973).

[89] A. Bramon, E. Etim, and M. Greco, Physics Letters B **41**, 609 (1972).

[90] R. Shankar, Phys. Rev. D **15**, 755 (1977).

[91] P. Gubler and D. Satow, Prog. Part. Nucl. Phys. **106**, 1 (2019).

[92] J. N. Ho, Beyond the conventional quark model: Using qcd sum rules to explore the spectrum of exotic hadrons, `https://harvest.usask.ca/bitstream/handle/10388/12979/HO-DISSERTATION-2020.pdf`, 2020.

[93] L. J. Reinders, S. Yazaki, and H. Rubinstein, Phys. Rep. **127**, 1 (1984).

[94] T. G. Steele and D. Harnett, arXiv e-prints , hep (2001).

[95] Y. Li and W. S. Gray, The formal laplace-borel transform, fliess operators and the composition product, in *Thirty-Sixth Southeastern Symposium on System Theory, 2004. Proceedings of the*, pp. 333–337, IEEE, 2004.

[96] O. Costin, *Asymptotics and Borel summability* (CRC press, 2008).

[97] R. A. Bertlmann, G. Launer, and E. de Rafael, Nucl. Phys. B **250**, 61 (1985).

[98] S. Groote, Electronic mail correspondence, 2021.

[99] G. S. Bali, C. Bauer, and A. Pineda, Phys. Rev. Lett. **113**, 092001 (2014).

[100] J. Ho, R. Berg, T. Steele, W. Chen, and D. Harnett, Physical Review D **100** (2019).

[101] S. Narison and E. de Rafael, Physics Letters B **103**, 57 (1981).

[102] T. G. Steele, K. Kostuik, and J. Kwan, Phys. Lett. B **451**, 201 (1999).

[103] R. T. Kleiv, T. G. Steele, A. Zhang, and I. Blokland, Physical Review D **87** (2013).

[104] J. Mathews, *Mathematical methods of physics*, 2d ed. ed. (The Benjamin Cummings, New York, W. A. Benjamin, 1970).

[105] A. Erdelyi, W. Magnus, F. Oberhettinger, and F. G. Tricomi, *Tables of Integral Transforms: Vol.: 2* (McGraw-Hill Book Company, Incorporated, 1954).

[106] D. D. H. Kaden Ray, Radiative corrections to the light 0^{++} tetraquark correlator using the numerical integrator pysecdec, in *University of Fraser Valley, Poster Competition*, 2019.

[107] S. Borowka, G. Heinrich, S. Jahn, S. Jones, M. Kerner, J. Schlenk, and T. Zirke, Comput. Phys. Commun. **222**, 313 (2018).

Appendix

Appendix A

This Appendix contains some theoretical details about the baseline algebra as well as some insights about tetraquarks and the construction of the famous light scalar nonet.

A.1: Conventions.

The Einstein summation is used implicitly. Here, some examples:

A $N-$dimension vector $\mathbf{v}$ will be written as a sum of their components x_i projected onto the basis vector of the system $\mathbf{e}_i$:

$$\mathbf{v} = \sum_{i=1}^{N} x_i \mathbf{e}_i \qquad \text{Einstein notation ignores the summation sign} \quad \rightarrow \quad \mathbf{v} = x_i \mathbf{e}_i, \tag{A.1}$$

where the summation over i is implied. This is extended to the matrix expressions, where each entry in a $M \times N$ matrix will be written as: c_{ij} where i, j runs from $1...M, N$, respectively. Hence, the product will be written as an implicit sum:

$$b_\nu = \sum_{\mu}^{N} a_{\nu\mu} c_\mu \qquad \rightarrow \text{ Einstein Notation } \rightarrow \qquad b_\nu = a_{\nu\mu} c_\mu. \tag{A.2}$$

In addition, the Minkowski space metric tensor $g^{\mu\nu}$ used is:

$$g^{\mu\nu} = \begin{pmatrix} 1 & 0 & 0 & 0 \\ 0 & -1 & 0 & 0 \\ 0 & 0 & -1 & 0 \\ 0 & 0 & 0 & -1 \end{pmatrix}. \tag{A.3}$$

The chiral representation of the 4-dimensional Dirac matrices is given by:

$$\gamma^0 = \begin{pmatrix} 0 & \mathbf{1} \\ \mathbf{1} & 0 \end{pmatrix}, \qquad \gamma^i = \begin{pmatrix} 0 & \sigma^i \\ -\sigma^i & 0 \end{pmatrix}, \tag{A.4}$$

where $\mathbf{1}$ is the 2×2 identity matrix, and σ^i are the Pauli matrices:

$$\sigma^1 = \begin{pmatrix} 0 & 1 \\ 1 & 0 \end{pmatrix}, \qquad \sigma^2 = \begin{pmatrix} 0 & -i \\ i & 0 \end{pmatrix}, \qquad \sigma^3 = \begin{pmatrix} 1 & 0 \\ 0 & -1 \end{pmatrix}. \tag{A.5}$$

A.2: Hadronic states.

The scalar nonet is expected to be a superposition of states, in which case all the possible outcomes that satisfy the requirements are allowed and in principle there is no need to choose a particular substructure. Hence, the states can be represented by [77]:

$$N_a^b \sim q_a \bar{q}^b, \qquad N_a^b \sim T_a \bar{T}^b,$$

where a possibility could be:

$$T_a = \epsilon_{abc} \bar{q}^b \bar{q}^c, \qquad \bar{T}^a = \epsilon_{abc} q_b q_c,$$

and a, b, $c = 1, 2, 3 = u$, $d\,s$. This is called the non-ideal mixing. Later, the state will be written as

$$|\Lambda\rangle = C_1 |q\bar{q}\rangle + C_2 |qq\bar{q}\bar{q}\rangle + C_3 \langle q\bar{q}q\bar{q}\rangle \ldots, \tag{A.6}$$

where C_1, C_2 and $\ldots$ are the weights of the function. The predictions will show then if the situation is closer to one type of substructure or another.

A.3: The lightest nonet.

The composition of the states are proposed to have the following structure:

$$\sigma = [ud][\bar{u}\bar{d}], \qquad f_0 = \frac{1}{\sqrt{2}}\big([su][\bar{s}\bar{u}] + [sd][\bar{s}\bar{d}]\big),$$
$$a_0 = \frac{1}{\sqrt{2}}\big([su][\bar{s}\bar{u}] - [sd][\bar{s}\bar{d}]\big), \qquad a_0^- = [sd][\bar{s}\bar{u}],$$
$$a_0^+ = [su][\bar{s}\bar{d}], \qquad \kappa^0 = [su][\bar{u}\bar{d}],$$
$$\bar{\kappa}^0 = [ud][\bar{s}\bar{u}], \qquad \kappa^- = [sd][\bar{u}\bar{d}],$$
$$\kappa^+ = [ud][\bar{s}\bar{d}].$$

Let us recall that the properties of Fig. 1.4 are obtained using the Gell-Mann-Nishijima formula:

$$Q = I_3 + \frac{Y}{2}, \tag{A.7}$$
$$I_3 = \frac{1}{2}(n_u - n_d), \tag{A.8}$$
$$Y = \frac{1}{3}(n_u + n_d - n_s), \tag{A.9}$$

where the I_3 is the third component of the Isospin and Y corresponds to the hypercharge; and n_u, n_d and n_s the number of up, down and strange quarks, respectively.

Appendix B

What about the complex analysis involved? This section shows sort of of a brief overview of the main mathematical tools used during the calculations.

B.1: The spectral function from the correlator.

On the one side, the QCD correlation function must be analytic, which happens to be in the whole range of the complex q^2-plane, except for the positive real axis, where the singularities are and where the phenomenology is studied. This issue is fixed by slightly shifting the

energy s with a $i\epsilon$ term in the vicinity of the real axis, from where complex analysis enter into the game.

From Fig. 2.3 one can separate the integral in the way mentioned in Eq. (2.8) and make use of the Schwarz reflection principle, which states $F(\bar{z}) = \overline{F(z)}$, hence

$$\Pi(s+i\epsilon) - \Pi(s-i\epsilon) = \Pi(s+i\epsilon) - \overline{\Pi(s+i\epsilon)} = 2i\mathrm{Im}\Pi(s+i\epsilon), \tag{A.10}$$

finally resulting in

$$\Pi(q^2) = \frac{1}{2i\pi}\int_{|s|=r} ds\,\frac{\Pi(s)}{s-q^2} + \frac{1}{\pi}\int_{t_0}^{r} ds\,\frac{\mathrm{Im}\Pi(s+i\epsilon)}{s-q^2}, \tag{A.11}$$

where the spectral function will be defined as:

$$\rho(s) = \frac{1}{\pi}\mathrm{Im}\Pi(s) \;\rightarrow\; \rho^{\mathrm{had}}(s) = \frac{1}{\pi}\mathrm{Im}\Pi^{\mathrm{QCD}}(s). \tag{A.12}$$

Later, with $r \to \infty$ the correlator will be written as:

$$\Pi(q^2) = \frac{1}{\pi}\int_{t_0}^{\infty} ds\,\frac{\rho^{\mathrm{had}}(s)}{s-q^2}. \tag{A.13}$$

B.2: Borel and Laplace transformations.

This section is intended to demonstrate the relation between the Borel transform operator and the inverse Laplace transform operator applied to the correlation function. Let us begin with the Borel operator, if we define the correlation function in the following way:

$$\Pi(Q^2) = \int_0^{\infty} \mathrm{d}s\,\frac{\rho(s)}{s+Q^2},$$

which will be transformed into

$$(-1)^n\,Q^{2n}\,\Pi(Q^2) = (-1)^n\,Q^{2n}\int_0^{\infty} \mathrm{d}s\,\frac{\rho(s)}{s+Q^2} = \int_0^{\infty} \mathrm{d}s\,(-1)^n\,Q^{2n}\,\frac{\rho(s)}{s+Q^2}. \tag{A.14}$$

Notice that we are able to do this since the integral is taken with respect to s, hence $(-1)^n Q^{2n}$ behaves as a multiplication factor. Later, applying the Borel transform operator:

$$\hat{B}\big[(-1)^n Q^{2n}\Pi(Q^2)\big] = \int_0^\infty \mathrm{d}s\, \hat{B}\Big[(-1)^n\, Q^{2n}\, \frac{\rho(s)}{s+Q^2}\Big] = \int_0^\infty \mathrm{d}s\, \rho(s)\, \hat{B}\Big[\, \frac{(-1)^n\, Q^{2n}}{s+Q^2}\Big]. \quad \text{(A.15)}$$

This equivalence holds because of the independence of the Borel transform on the spectral function $\rho(s)$, since the relation we are aiming to do is between Q^2 and τ. Now we are able to use the properties of the Borel transform operator mentioned in Eq. (2.17) in Chapter 2.

$$\hat{B}\big[(-1)^n Q^{2n}\Pi(Q^2)\big] = \int_0^\infty \mathrm{d}s\, \rho(s)\, (-1)^n \Big\{(-1)^n\, s^n \tau \mathrm{e}^{-s\tau}\Big\}. \quad \text{(A.16)}$$

Finally,

$$\frac{1}{\tau}\hat{B}\big[(-1)^n Q^{2n}\Pi(Q^2)\big] = \int_0^\infty \mathrm{d}s\, \rho(s)\, s^n \mathrm{e}^{-s\tau}. \quad \text{(A.17)}$$

On the other hand, we can look at the Laplace transform applied to the same expression:

$$\mathcal{L}^{-1}\big[(-1)^n Q^{2n}\Pi(Q^2); \tau\big] = \mathcal{L}^{-1}\left[\int_0^\infty \mathrm{d}s\, \frac{(-1)^n Q^{2n}\rho(s)}{s+Q^2}; \tau\right] \quad \text{(A.18)}$$

Notice that the Laplace transform does not affect the integral, since again, this transformation is relating Q^2 with τ. Here, we can use the Laplace transform properties (see e.g. Refs. [104, 105]):

$$\mathcal{L}\left[\alpha\, g(x) + \beta\, h(x);\, y\right] = \alpha\, \mathcal{L}\left[g(x);\, y\right] + \beta\, \mathcal{L}\left(h(x);\, y\right), \qquad \alpha, \beta \text{ are constants,} \quad \text{(A.19)}$$

$$\mathcal{L}\left[x^n\, g(x);\, y\right] = (-1)^n\, \frac{\mathrm{d}^n}{(\mathrm{d}y)^n} \mathcal{L}\left[g(x);\, y\right]. \quad \text{(A.20)}$$

(More information about this relation can be found in Refs. [83, 95–97].) Now, we can look at Eq. (A.18) and move to the complex Q^2-plane, this can be rewritten as:

$$\mathcal{L}^{-1}\left[(-1)^n Q^{2n}\, \Pi(Q^2);\, \tau\right] = \int_0^\infty \mathrm{d}s\, \rho(s)\, \mathcal{L}^{-1}\left[\frac{(-1)^n Q^{2n}}{s+Q^2};\, \tau\right]. \quad \text{(A.21)}$$

Focusing our attention on the Laplace inverse transform, using its definition based on complex analysis by invoking the Cauchy theorem, and replacing $Q^2 = z$, where $z \, \epsilon \, \mathbb{C}$, this expression becomes:

$$\mathcal{L}^{-1}\left[\frac{(-1)^n Q^{2n}}{s+Q^2};\, \tau\right] = \mathcal{L}^{-1}\left[\frac{(-1)^n z^n}{s+z};\, \tau\right] = \frac{(-1)^n}{2\pi i}\int_{c-i\infty}^{c+i\infty} \mathrm{d}z\, \frac{z^n\, \mathrm{e}^{z\tau}}{s+z}. \tag{A.22}$$

It is straightforward to see that Eq. (A.22) has a simple pole at $z = -s$, with can be solved by making use of the Residue Theorem:

$$\oint_C f(z)\, \mathrm{d}z = 2\pi i \, \{Res \; at \; z = -s\}. \tag{A.23}$$

Resulting in,

$$\oint_C \frac{z^n \mathrm{e}^{z\tau}}{z+s} = (-1)^n s^n \mathrm{e}^{-s\tau}. \tag{A.24}$$

Finally, establishing the equivalence of Eq. (A.17) and the following expression

$$\mathcal{L}^{-1}\big[(-1)^n Q^{2n} \Pi(Q^2); \tau\big] = \int_0^\infty \mathrm{d}s\, \rho(s)\, s^n \mathrm{e}^{-s\tau}. \tag{A.25}$$

Appendix C

This section is devoted to show the preliminary work done before the final QCD sum-rule analysis.

C.1: Pseudoscalar tetraquark current.

The aim of the preliminary work was focused on developing the skills working with `MATHEMATICA` and understanding the structure of the currents, the correlator for tetraquark systems and their spectral densities.

The first task was oriented in the comparison of two studies of the NLO contributions of the perturbative term of the light-tetraquark correlator based on the current $J^{\sigma}_{P_6}$ [11, 106].

The calculations in the studies were formulated using different techniques, i.e., their

framework was different but the results can still be compared due to its definition of the object of study, which is the pseudoscalar flavour symmetric current correlation function. The first article studied (see Ref. [11]) computed the spectral function in $x-$space and transformed to $p-$space at the very end, whereas the other study (see Ref. [106]) was made purely in $p-$space via numerical loop calculations with pySecDec (Python Sector Decomposition [107]). In principle, the comparison can give us a clue on which could be the aspects to consider in the calculations, whether they agree or not and how to make a proper interpretation of these results, plus this task helps to have better understanding of the structure of light-tetraquark systems.

To begin with, the definition of the correlator shown in Eq. (2.6) using the pseudoscalar flavour symmetric current (Eq. (A.26)) must be defined. For simplicity, the current will be reduced to

$$J(x)^{\sigma}_{P_6} = \delta^k_i\, \delta^l_j \left(q^{i\mathrm{T}}(x)\, C\, q^j(x) \right) \left(\overline{q}_k(x)\, C\, \overline{q}^{\mathrm{T}}_l(x) \right), \tag{A.26}$$

where the indices i, j, k, l indicate the quark flavour.

In the approach taken by Ref. [11], the correlator was built considering a set of ingredients, such as the quarks as propagator and dipropagator and their corresponding NLO corrections. Fig. A.1 illustrates this idea by showing the Feynman diagrams of each case.

(a) **(b)**

Figure A.1: Feynman diagrams of the LO and NLO of the propagator.

Using the so-called Feynman rules to compute the correlator from previously defined

Figure A.2: Feynman diagrams of the LO and NLO of the dipropagator.

currents, we are able to extract the loop integrals from these diagrams, being the following[1]:

$$I_{(a)} = \int \frac{d^D q}{(2\pi)^D} \left(\frac{i}{\not q}\right), \tag{A.27}$$

$$I_{(b)} = \int \frac{d^D k}{(2\pi)^D} \left(\frac{i}{\not q}\right) \left[-i\tilde{g}_s \gamma^\alpha T_a\right] \left(\frac{i}{\not k}\right) \left[-i\tilde{g}_s \gamma^\beta T_b\right] \frac{-i g_{\alpha\beta}\delta_{ab}}{(q-k)^2} \left(\frac{i}{\not q}\right), \tag{A.28}$$

$$I_{(c)} = \int \frac{d^D k}{(2\pi)^D} \left(\frac{i}{\not k} \otimes \frac{i}{\not q - \not k}\right), \tag{A.29}$$

$$I_{(d)} = \int \frac{d^D k}{(2\pi)^D} \frac{d^D l}{(2\pi)^D} \left(\frac{i}{\not k}\right) \left[-i\tilde{g}_s \gamma^\alpha T_a\right] \left(\frac{i}{\not l}\right) \otimes \left(\frac{i}{\not q - \not k}\right) \left[-i\tilde{g}_s \gamma^\beta T_b\right] \left(\frac{i}{\not q - \not l}\right) \frac{-i g_{\alpha\beta}\delta_{ab}}{(k-l)^2}. \tag{A.30}$$

From these equations the correlation functions were computed using dimensional regularization and renormalization methods (see Ref. [11] for further details).

C.2: Correlation function of pseudoscalar currents.

Later, the spectral functions were obtained in terms of the parameter ϵ that arises from dimensional regularization, and it is defined as $D = 4 - \epsilon$ with $\epsilon \to 0$ and the renormalization scale $\mu^2_{\overline{MS}}$ in the modified minimal subtraction scheme,

$$\rho_{\rm LO}(s,\epsilon) = s^4 \left[\frac{A_0}{\epsilon} + A_1 + A_2\epsilon\right], \tag{A.31}$$

$$\rho_{\rm NLO}(s,\mu,\epsilon) = s^4 \left(\alpha + \beta \log \frac{s}{\mu^2_{\overline{MS}}}\right) \left[\frac{B_0}{\epsilon} + B_1 + B_2\epsilon\right], \tag{A.32}$$

[1]The strong coupling here has mass dimensions, but this is absorbed with the renormalization scale [11].

where α and β contain the strong coupling constant $\alpha_s(\mu^2_{\overline{MS}})$ inherent from the gluon exchange diagrams. Now, the terms to be compared are the ones proportional to ϵ^0 and after merging all the constants, the spectral function reduces to

$$\rho(s,\mu) = As^4 + B\alpha_s s^4 + C\alpha_s s^4 \log\left(\frac{s}{\mu^2}\right) = \overbrace{A\,s^4}^{LO} + \underbrace{Bs^4 + Cs^4 \log\left(\frac{s}{\mu^2}\right)}_{NLO}, \tag{A.33}$$

where the A, B and C are the coefficients of the polynomials, and the strong coupling is hidden in B and C.

C.3: Comparison of results.

In order to compare properly both studies [11, 19, 106], the renormalization scale parameter was taken to be a fixed value $\mu^2_{\overline{MS}} = 1\,GeV^2$ and the strong coupling constant was adjusted at this scale. To begin with, the results of the first study, Ref. [11], are

$$\rho(s) = \frac{2s^4}{15(4\pi)^6}\left\{1 + \frac{3\alpha_s}{10\pi} + \frac{\alpha_s}{\pi}\log\left(\frac{s}{\mu^2_{\overline{MS}}}\right)\right\}. \tag{A.34}$$

Likewise, I obtained these polynomial coefficients of the other study, Ref. [106], taking the numerical results for the imaginary part of the correlator and fitting the curves by sector, i.e., considering the contribution from each diagram. The plots shown in Fig. A.3 display how data is presented separated by the real (LHS) and imaginary part (RHS) and by contributions of the powers of ϵ (from ϵ^{-1} on top to ϵ at the bottom).

In the LO case, the curve was fitted by the function As^4, while the NLO corrections were fitted by the corresponding function resulting from the NLO terms of Eq. (A.33), extracting B and C per each diagram and summing them to compute the spectral function. The results obtained for the coefficients are shown in the following table.

Even though the LO coefficients are in agreement for both studies, the NLO contributions do not and their difference is remarkable, since they differ by at least one order of magnitude. A closer analysis of Ref. [106] is needed to resolve this discrepancy. However, both studies are showing a significant contribution from the NLO corrections to the spectral function and

Coefficients	Groote et.al. Ref. [11]	D. Harnett Ref. [106]
A	3.3859×10^{-8}	3.39022×10^{-8}
B	1.4652×10^{-9}	2.5506×10^{-7}
C	-4.8839×10^{-9}	-1.4372×10^{-8}

Table A.1: Coefficients of the polynomial of Eq. (A.33)

this behaviour is represented clearly in Fig. A.4.

From this comparison is also important to mention that the approach taken, either from coordinate space or from momentum space, must include all the possible constants and factors associated with colour and from the renormalization procedure.

Finally, from this analysis we are able to elucidate the large contribution from NLO diagrams to the spectral functions, giving us the needed clue to estimate the size of the contribution to the sum rules.

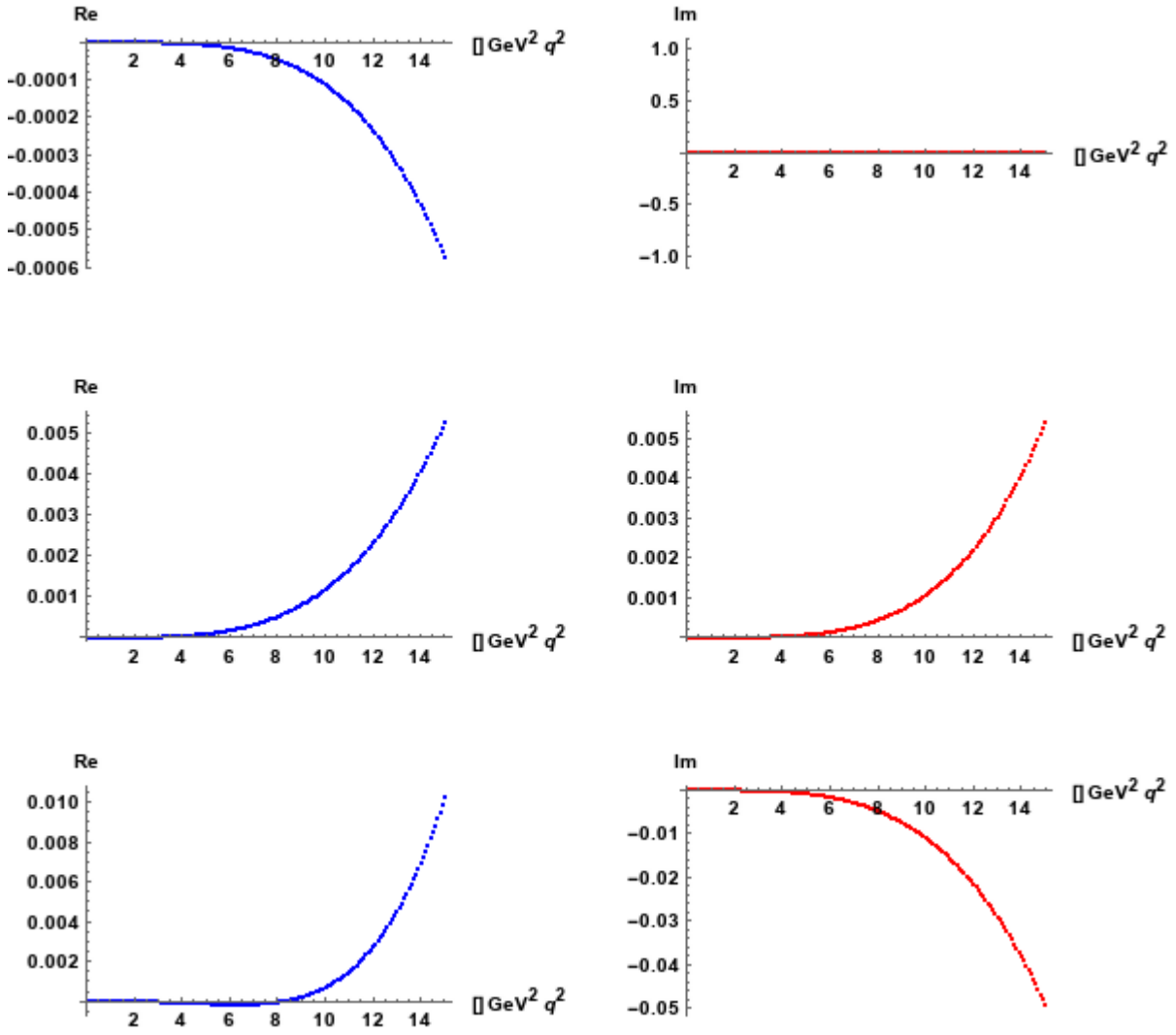

Figure A.3: LO correlation function obtained from the numerical pySecDec calculations.

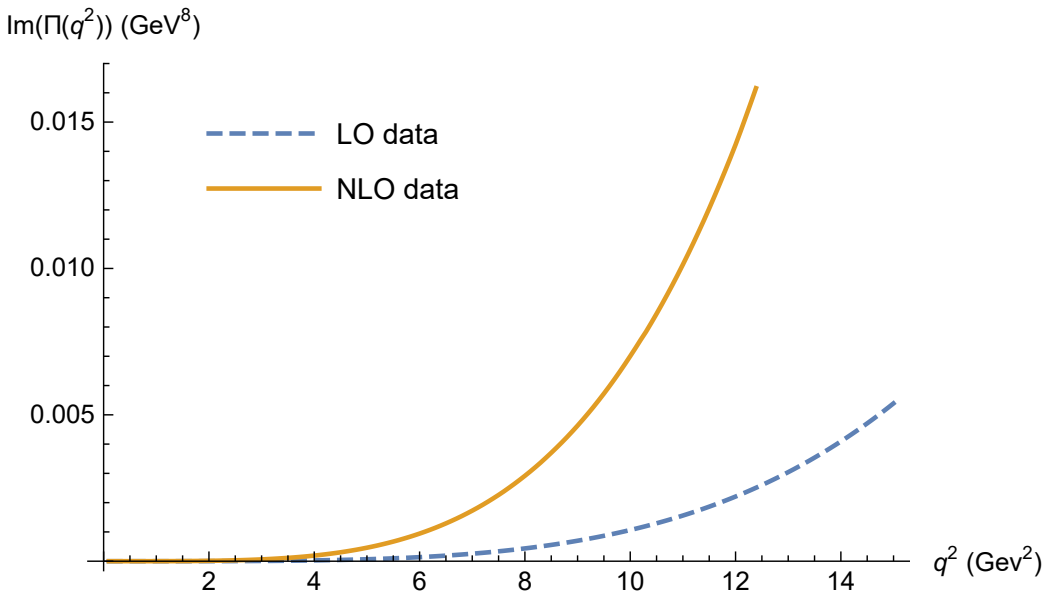

Figure A.4: LO and NLO contributions to the pseudoscalar correlation function.